

J 14

SINGULAR PERTURBATION ANALYSIS OF AOTV-RELATED TRAJECTORY OPTIMIZATION PROBLEMS - FINAL REPORT

January, 1990

**Research Supported by
NASA Langley Research Center
Grant No. NAG-1-660**

**Principal Investigator: Dr. Anthony J. Calise
Research Assistant: Dr. Gyoung H. Bae
NASA Grant Monitors: Dr. Christopher Gracey
Dr. Daniel D. Moerder**

**Georgia Institute of Technology
School of Aerospace Engineering
Atlanta, GA 30332**

SINGULAR PERTURBATION ANALYSIS OF AOTV-RELATED TRAJECTORY OPTIMIZATION PROBLEMS

Anthony J. Calise
Georgia Institute of Technology
School of Aerospace Engineering
Atlanta, GA 30332

SUMMARY

This research has addressed the problem of real time guidance and optimal control of Aeroassisted Orbit Transfer Vehicles (AOTV's), using singular perturbation theory as an underlying method of analysis. Trajectories have been optimized with the objective of minimum energy expenditure in the atmospheric phase of the maneuver. Two major problem areas were addressed: optimal reentry, and synergetic plane change with aeroglide. For the reentry problem, several reduced order models were analyzed with the objective of optimal changes in heading with minimum energy loss. It has been demonstrated that a further model order reduction to a single state model is possible through the application of singular perturbation theory. The optimal solution for the reduced problem defines an optimal altitude profile dependent on the current energy level of the vehicle. A separate boundary layer analysis is used to account for altitude and flight path angle dynamics, and to obtain lift and bank angle control solutions. By considering alternative approximations to solve the boundary layer problem, three guidance laws were derived, each having an analytic feedback form. The guidance laws were evaluated using a Maneuvering Reentry Research Vehicle model and all three were found to be near optimal.

For the problem of synergetic plane change with aeroglide, a difficult terminal boundary layer control problem arises which to date has been found to be analytically intractable. Thus a predictive/corrective solution was developed to satisfy the terminal constraints on altitude and flight path angle. A composite guidance solution was obtained by combining the optimal reentry solution with the predictive/corrective guidance method. Numerical comparisons with the corresponding optimal trajectory solutions show that the resulting performance is very close to optimal.

An attempt was made to obtain numerically optimized trajectories for the case where heating rate is constrained. A first order state variable inequality constraint was imposed on the full order AOTV point mass equations of motion, using a simple aerodynamic heating rate model. For high heating rate limits (just below the peak heating rate for the unconstrained case), the resulting solution appears to satisfy the first order necessary conditions for a "touch point" problem, where the constraint is met at a single point. Lower heating rate limits likely result in a constrained arc, of finite duration. Unfortunately, numerically converged optimal trajectories for this range of solutions could not be obtained using the multiple shooting method employed in this research.

TABLE OF CONTENTS

	<u>Page</u>
Section 1 - Introduction	1
Section 2 - Problem Formulation	3
2.1 Equations of Motion	3
2.2 Singular Perturbation Formulation	5
2.3 Boundary Conditions	7
Section 3 - Heading Change With Minimum Energy Loss	8
3.1 Singular Perturbation Analysis	9
3.2 Numerical Results	14
Section 4 - Aeroassisted Orbit Transfer	17
4.1 Guidance During the Reentry Phase	18
4.2 Guidance During the Exit Phase	18
4.3 Numerical Results	19
Section 5 - Constrained Aeroglide	21
5.1 Problem Formulation	21
5.2 Numerical Results	21
Section 6 - Conclusions and Recommendations	23
6.1 Conclusions	23
6.2 Recommendations	24
6.3 Publications	25
References	26

LIST OF FIGURES

	<u>Page</u>
Figure 1. Comparison of the reduced solution altitude profile with an optimal profile for a 40° heading change.	28
Figure 2. Comparison of the SP1 and SP3 guided altitude profiles with the reduced solution	29
Figure 3. Comparison of the SP2 guided altitude profile with the reduced solution.	30
Figure 4. Comparison of the guided altitude profiles with the true optimal solution	31
Figure 5. Bank angle profiles	32
Figure 6. Normalized lift coefficient profiles.	33
Figure 7. Heading profiles.	34
Figure 8. Depiction of the exit phase maneuver.	35
Figure 9. Guided solution altitude profiles	36
Figure 10. Guided solution bank angle profiles	37
Figure 11. Optimal solution altitude profiles.	38
Figure 12. Optimal solution bank angle profiles.	39
Figure 13. Optimal solution normalized lift coefficient profiles.	40
Figure 14. Altitude profiles for the unconstrained and touch point solutions	41
Figure 15. Velocity profiles for the unconstrained and touch point solutions	42
Figure 16. Inclination angle profiles for the unconstrained and touch point solutions	43
Figure 17. Normalized lift coefficient profiles for the unconstrained and touch point solution.	44
Figure 18. Bank angle profiles for the unconstrained and touch point solutions	45
Figure 19. Altitude costate profiles for the unconstrained and touch point solutions	46
Figure 20. Velocity costate profiles for the unconstrained and touch point solutions	47

LIST OF TABLES

	<u>Page</u>
Table 1	Comparison of Final Energies for the Reentry Problem. . . . 48
Table 2	Comparison of Energy Loss for the AOTV Problem. 48

SECTION 1

INTRODUCTION

Energy state approximations combined with singular perturbation theory have proven useful in aircraft trajectory optimization, both in obtaining algebraic control solutions and in satisfying trajectory and control constraints [1-4]. However, the underlying flat earth and constant gravitational field assumptions in aircraft modeling do not apply to hypersonic vehicles. Moreover, the use of singular perturbation theory requires an inherent time scale separation in the problem formulation for successful application. The intent of this research effort has been to explore the usefulness of singular perturbation analysis in the development of real time guidance algorithms for problems related to AOTV maneuvers.

The problem of optimal atmospheric heading change with minimum energy loss has application to maneuvering reentry vehicle guidance and to aeroassisted orbit transfer vehicle (AOTV) guidance. The problem of aeroassisted orbit plane change requires the use of three impulses - one to deorbit, one to reorbit and one to recircularize at the new orbit. The orbit plane change is effected entirely in the atmosphere through the use of lift and bank angle control. Circular orbit plane changes in which the initial and final orbital altitudes are equal were studied in [5-9]. These studies considered various problem formulations with the underlying approximation that an expression related to the sum of the centrifugal and gravitational forces (Loh's term) is constant or piecewise constant over the atmospheric maneuver. Furthermore, in the absence of heating constraints, the optimal trajectories are of short duration, and the inclination change is closely approximated by the heading change. For this situation, the dynamics can be reduced to fourth order, and minimization of fuel consumption is closely approximated by minimizing the energy loss in the atmospheric portion of the trajectory [6]. As a point of reference, the optimal AOTV maneuver requires approximately 50% of the fuel needed for the single impulse pure propulsive maneuver in the case of a 40 degree low Earth orbit plane change. In [10], a regular perturbation method is used to remove the approximations related to Loh's term in the earlier work and demonstrates a significant improvement over the solutions in [5-9]. However, this approach requires a quadrature at

each update of the control solution and the approach can not be readily extended to include the effect of heating constraints.

Examples of numerical optimization studies related to orbit plane change can be found in [11-13]. In particular, [12-13] examine the effect of a heating rate constraint with thrusting in the atmosphere. Since the duration of the AOTV maneuver is much greater when a heating rate constraint is enforced, it is necessary to consider a more complete set of dynamics which includes the cross range angle. Ref. [12] treats the problem of optimal aerocruise (flight at constant altitude and velocity), and does not consider the transitions to and from the cruise condition. In [13], a more general problem is treated with a constant thrust segment inserted during the atmospheric phase. Thus, in our work we decided to place emphasis on optimal aeroglide (no thrusting in the atmosphere) subject to a heating rate constraint. A more complete account of related work in noncoplanar transfer, including other competing transfer modes, can be found in [14].

Section 2 of this report presents the problem formulation and issues related to model order reduction. Section 3 treats the problem of optimal heading change with minimum energy loss in the context of singular perturbation analysis. Section 4 addresses the AOTV synergetic plane change problem by introducing a predictive/corrective solution to satisfy the terminal constraints on altitude and flight path angle. Section 5 summarizes the results for a numerical study of the effects of a heating rate constraint on the AOTV synergetic plane change problem. Section 6 summarizes the results and recommendations for further research along this line.

SECTION 2
PROBLEM FORMULATION

2.1 Equations of Motion

The equations of motion for gliding flight about a spherical nonrotating Earth are given by:

$$d\theta/dt = V\cos\gamma\cos\psi/r\cos\phi: \quad r = r_s + h \quad (1)$$

$$d\phi/dt = V\cos\gamma\sin\psi/r \quad (2)$$

$$dh/dt = V\sin\gamma \quad (3)$$

$$dV/dt = -D/m - g\sin\gamma: \quad g = v/r^2 \quad (4)$$

$$Vd\gamma/dt = L\cos\mu/m + (V^2/r - g)\cos\gamma \quad (5)$$

$$Vd\psi/dt = L\sin\mu/m\cos\gamma - (V^2/r)\cos\gamma\cos\psi\tan\phi \quad (6)$$

where θ is the longitude, ϕ is the latitude, h is the altitude, r_s is the Earth's radius, V is the velocity, γ is the flight path angle, ψ is the heading angle, D is the drag force, v is the Earth's gravitational constant, and m is the vehicle mass. The control variables are the lift force (L) and bank angle (μ).

The orbit inclination angle is given by the relation

$$\cos i = \cos\phi\cos\psi \quad (7)$$

The plane change is the angle between the normals to the initial and final orbital planes. The actual inclination (i) is defined relative to the equatorial plane. Many studies on optimal plane change have taken the equatorial plane as the initial plane, in which case the plane change equals the final inclination angle (i_f). However, it has been shown in [12] that, under the assumption of spherical symmetry, maximizing the inclination is equivalent to maximizing the plane change angle provided that the deorbit burn is properly timed so that the plane change occurs at the proper location. This depends only on the location of the ascending node for the final orbit plane.

Thus, there is no loss in generality in assuming that the initial plane is the equatorial plane, and that the inclination change is the final inclination angle. A second consequence of this fact is that θ becomes an ignorable coordinate in most AOTV optimization problems since it does not appear in the right hand side of the equations of motion, and it does not enter the boundary conditions or the performance index for optimal control problem formulations of practical interest.

For short duration maneuvers, the cross range angle can be treated as being negligibly small in (1),(6) and (7). In this case the inclination change is approximated by the heading change, and ϕ also becomes an ignorable coordinate. Thus it is possible to reduce the equations of motion to a four state model, which for the purposes of this study are expressed in the following form:

$$dh/dt = V \sin \gamma \quad (8)$$

$$dE/dt = -C_D^* S (1 + \lambda^2) \rho V^3 / 4m \quad (9)$$

$$d\gamma/dt = (C_L^* \rho S V / 2m) (\lambda \cos \mu + M \cos \gamma) \quad (10)$$

$$d\psi/dt = C_L^* \lambda \rho S V \sin \mu / 2m \cos \gamma \quad (11)$$

where

$$C_D = C_{D0} + K C_L^2 \quad (12)$$

$$M(h, V) = (2m / C_L^* S) [1 - v / V^2 r] / \rho r, \quad r = r_s + h \quad (13)$$

In these equations the superscript * denotes the maximum lift-to drag values:

$$C_L^* = (C_{D0} / K)^{1/2} \quad C_D^* = 2C_{D0} \quad (14)$$

and λ is the normalized lift coefficient

$$\lambda = C_L / C_L^* \quad (15)$$

Here we have employed E as a state variable in place of velocity (V), where

$$E = V^2/2 - v/r \quad (16)$$

In [6] velocity is used as a state variable, and the gravity component was ignored in the velocity rate equation. One advantage to using E as a state variable is that (9) is independent of γ . In (16), the reference point for zero potential energy is taken at $r = \infty$. This transformation implies that wherever V appears in the equations, it is replaced by $[2(E+v/r)]^{1/2}$. The control variables are λ and the bank angle (μ). Under the hypothesis that the cross range angle is small, ψ closely approximates the change in orbit inclination.

A further reduction to a third order model is justifiable if the objective is minimize the energy loss in the atmospheric phase of the maneuver. In this case one can treat energy as constant in the dynamics, and account for the energy loss in the performance index using the following integral form

$$J = \int_0^{t_f} C_D S (1+\lambda^2) \rho V^3 / 4m \, dt \quad (17)$$

Thus, E can also be regarded as an ignorable coordinate in this case. This will result in a reasonable approximation if the energy loss is small compared to the total vehicle energy. This approximation is greatly improved if the control solution is periodically updated to account for the present vehicle energy during the maneuver, which would be the case if a feedback (analytic) optimal control solution form was obtainable.

2.2 Singular Perturbation Formulation

The main approximation introduced here is that altitude and flight path angle dynamics can be regarded as fast compared to heading dynamics. In the context of singular perturbation theory, this implies a further order reduction to a single state model, with altitude as the control variable. To motivate this viewpoint, it is desirable to identify a small parameter which

appears as a multiplying factor on the left side of the altitude and flight path angle equations of motion. Currently, there is no systematic procedure for putting the equations of motion in this standard form. However, it is generally agreed that the equations of motion should always be non-dimensionalized as an initial step. The following transformations are introduced here to justify the formulation adopted in this study.

Define the following non-dimensional variables:

$$\psi_1 = \psi/\psi_f \quad t_1 = (C_L^* S \rho_0 V_C / 2m\psi_f)t \quad (18)$$

$$V_1 = V/V_C \quad \rho_1 = \rho/\rho_0 \quad (19)$$

$$h_1 = h/h_0 \quad r_1 = r/r_0 \quad (20)$$

where h_0 is the entry altitude, ρ_0 is the air density at $h = h_0$, $V_C = [v/r_0]^{1/2}$ is the circular velocity at h_0 , and ψ_f is the final heading (final inclination for small changes in ϕ). Also assume that for the altitudes of interest that $r = r_s$. Then (9), (11-12) become:

$$d\psi_1/dt_1 = \rho_1 V_1 \lambda \sin\mu / \cos\gamma \quad (21)$$

$$\epsilon dh_1/dt_1 = V_1 \sin\gamma \quad (22)$$

$$\epsilon d\gamma_1/dt_1 = C_L S \rho V_C V_1 \lambda \cos\mu / 2m + V_C V_1 [1 - 1/V_1^2 r_s] \cos\gamma / r_s \quad (23)$$

where $\epsilon = C_L^* S \rho_0 h_0 / 2m\psi_f$. Hence ϵ is a small parameter for sufficiently large heading changes, or if

$$C_L^* S \rho_0 h_0 / 2m \ll \psi_f \quad (24)$$

A typical calculation for a 40° plane change and $h_0 = 200,000$ ft gives $\epsilon = 0.0043$ for a vehicle with a maximum L/D of 2.3.

The analysis in Section 3 of this report uses the original state variables and artificially introduces $\epsilon = 1.0$ as a scaling parameter. It can

be shown that this formal procedure results in the same control solution as that obtained using the formulation in (21-23) in the non-dimensionalized variables.

2.3 Boundary Conditions

In [6], the sensible atmosphere is assumed to occur at $h(0) = 200,000$ ft. The starting velocity and flight path angle are derived using a deorbit impulse ΔV_1 from circular orbit at $h_c = 100$ nm, which is optimized for the atmospheric maneuver of interest. The initial heading angle is taken as zero. In the singular perturbation formulation, altitude appears as a control variable in the reduced problem. The optimal solution appears in the form

$$\overset{*}{h} = h_0(E) \quad (25)$$

For comparison purposes, in this paper the starting energy is chosen to match that of [8] for the case of a 40° heading change. From conservation of energy this results in the same deorbit impulse. The initial flight path angle is derived from conservation of angular momentum.

$$\gamma(0) = -\cos^{-1}[(r_c)(V_c - \Delta V_1)/(r_s + h(0)V(0))] \quad (26)$$

where r_c is the circular orbit radius and $V_c = (v/r_c)^{1/2}$ is the circular velocity. The vehicle begins the maneuver with a mass m_c and, as a result of the deorbit impulse, the mass for the atmospheric portion is given by

$$m = m_c \exp(-\Delta V_1/C) \quad (27)$$

The terminal condition is taken as:

$$\psi(t_f) = \psi_f > 0 \quad (28)$$

For the reentry problem there are no terminal constraints on altitude and flight path angle, thus their corresponding costate values are zero at the final time. For the noncoplanar orbit transfer problem, the final altitude is constrained to ensure exit from the atmosphere.

SECTION 3
HEADING CHANGE WITH MINIMUM ENERGY LOSS

The objective is to minimize the energy lost in maneuvering to a specified heading. Regarding energy as a slow variable, and altitude and flight path angle as fast variables, the following three state model was adopted for singular perturbation analysis:

$$d\psi/dt = C_L^* \rho S V \lambda \sin\mu / 2m \cos\gamma \quad (29)$$

$$\epsilon dh/dt = V \sin\gamma \quad (30)$$

$$\epsilon \gamma/dt = C_L^* \rho S V (\lambda \cos\mu + M \cos\gamma) / 2m \quad (31)$$

The objective is to minimize

$$J = - \int_0^{t_f} \dot{E} dt \quad (32)$$

where

$$\dot{E} = -C_D^* (1 + \lambda^2) \rho S V^3 / 4m \quad (33)$$

Note that in the above formulation E is approximated as constant in the dynamics, but that changes in energy are accounted for in the performance index. This approximation will later be relaxed in the subsequent analysis. The perturbation parameter ϵ is introduced to signify the presence of fast dynamics, and is nominally equal 1.0. We seek a reduced and zero order boundary layer solution about $\epsilon = 0$, in accordance with the procedures detailed in [2-4]. Regarding h and γ as fast states is characteristic of energy state analysis for fighter and transport aircraft. Therefore, we adopt the same framework in this analysis. Considering both h and γ in the same time scale results in a two point boundary value problem. A feedback guidance law is obtained by expansion of the necessary conditions to first order [15]. In this regard, it should be noted that there have been some studies that have also considered analysis of h and γ dynamics on separate time scales [16], which avoids linearization the boundary layer dynamics. Therefore, an additional set of guidance laws are possible beyond those presented here.

3.1 Singular Perturbation Analysis

Reduced Problem

Setting $\epsilon = 0$ in (29-31) the necessary conditions for optimality become:

$$H_0 = \lambda_{\dot{\psi}} \dot{\psi} - \dot{E} = 0 \quad (34)$$

$$\gamma = 0, \quad \lambda \cos \mu = -M \quad (35)$$

$$\mu_0, h_0 = \arg \min_{h, \mu} \{\dot{\psi}/\dot{E}\} \quad (36)$$

It can be shown that this results in the following reduced solution:

$$\lambda_0 = (1 + 2M_0^2)^{1/2} \quad (37)$$

$$\sin \mu_0 = [(1 + M_0^2)/(1 + 2M_0^2)]^{1/2} \quad (38)$$

$$h_0 = \arg \min_h \{V^2 (1 + M^2)^{1/2}\} |_{E = \text{const.}} \quad (39)$$

where M_0 is the value of M for $h = h_0$. The quadrant for the bank angle in (38) is resolved based on the following inequalities:

$$0 < \mu_0 < \pi/2 \text{ for } M_0 < 0 \quad (40)$$

$$\pi/2 < \mu_0 < \pi \text{ for } M_0 > 0 \quad (41)$$

It can be seen from the above solution that M plays a crucial role in the solution process.

Since most of the energy is kinetic, V is weakly dependent on h for constant E . This can readily be seen from (16) where changes in h give rise to small changes in r . Thus, the minimization in (39) results in a value for M very close to zero. The interpretation is that the maneuver should be performed at an altitude where gravitational and centrifugal forces nearly

cancel one another. For M small, it can be seen from (37,38) that the maneuver is performed at near maximum L/D and at near 90° of bank angle. These results are in good agreement with the results in [6] for the AOTV problem. It will also be shown in Section 3.2 that the reduced solution altitude profile, $h_0(E)$, closely resembles the altitude profile of [6] for the case of large changes in inclination angle.

Boundary Layer Problem

Introducing the transformation $\tau = t/\varepsilon$ and again setting $\varepsilon = 0$, the necessary conditions in the boundary layer are:

$$H_{BL} = \lambda_{\psi}^0 \dot{\psi} + \lambda_h V \sin \gamma + \lambda_{\dot{\gamma}} \dot{\gamma} - \dot{E} = 0 \quad (42)$$

$$\partial H_{BL} / \partial L_1 = 0, \quad \partial H_{BL} / \partial L_2 = 0 \quad (43)$$

where λ_{ψ}^0 is determined in the reduced solution from (34)

$$\lambda_{\psi}^0 = \dot{E}^0 / \dot{\psi}^0 = -C_D^* V_0^2 (1 + M_0^2)^{1/2} / C_L^* \quad (44)$$

using the solutions for λ_0 , μ_0 and h_0 . In (43), L_1 and L_2 represent the horizontal and vertical components of lift coefficient

$$L_1 = \lambda \sin \mu \quad L_2 = \lambda \cos \mu \quad (45)$$

which are now used as control variables in place of λ and μ .

The first condition in (43) results in

$$L_1^* = (V_0/V)^2 (1 + M_0^2)^{1/2} / \cos \gamma \quad (46)$$

where M_0 , V_0 are the values of M and V corresponding to $h = h_0$ for the current value of E. This solution approaches the corresponding reduced solution as h approaches h_0 .

The second condition in (43) yields

$$L_2^* = -(C_L^*/C_D^* V^2) \lambda_\gamma \quad (47)$$

which can also be shown to approach the reduced solution as h approaches h_0 , where

$$\lambda_\gamma^0 = C_D^* V_0^2 M_0 / C_L^*, \quad \lambda_h^0 = 0 \quad (48)$$

The reduced solution for λ_γ in (48) follows immediately from (31) and (47) with $L_2^* = -M_0$ ($\dot{\epsilon}\dot{\gamma} = 0$, in the reduced solution). The second condition in (48) is a consequence of the fact that h_0 results from an unconstrained minimization of H^0 . Note that λ_h^0 satisfies the terminal boundary condition, but λ_γ^0 does not. This point will be addressed in the numerical results section.

Unfortunately, evaluation of λ_γ needed in (47) requires the solution of a two-point boundary value problem. When close to the reduced solution it may be possible to use (48), which results in the following expression for flight path angle rate

$$d\gamma/dt = C_L^* \rho S V (M \cos^2 \gamma - V_0^2 M_0 / V) / 2m \quad (49)$$

For γ near zero and h near h_0 , (49) simplifies to

$$d\gamma/dt = C_L^* \rho S V_0 (M - M_0) / 2m \quad (50)$$

Use of (46) and (47) with $\lambda_\gamma = \lambda_\gamma^0$ results in a guidance law in feedback form, which we denote as the "SP1" Solution.

Expansion of the Boundary Layer Problem [15]

A second feedback solution can be obtained by considering an expansion of the boundary layer necessary conditions of (42,43) together with the state and costate dynamics expressed in the stretched time scale $\tau = t/\epsilon$:

$$dh/d\tau = V \sin \gamma, \quad d\lambda_h/d\tau = -\partial H_{BL} / \partial h \quad (51)$$

$$d\gamma/d\tau = C_{L\rho}^* SV(L_2 + M\cos\gamma)/2m, \quad d\lambda\gamma/d\tau = -\partial H_{BL}/\partial\gamma \quad (52)$$

Substituting for L_1 and L_2 from (46,47), equations (51,52) are expanded about the reduced solutions equilibrium conditions:

$$\bar{h} = h_0(E), \quad \bar{\gamma} = 0 \quad (53)$$

$$\bar{\lambda}_h = 0, \quad \bar{\lambda}_\gamma = \lambda_\gamma^0 \quad (54)$$

This results in the following linear perturbation equations:

$$\begin{bmatrix} \delta h' \\ \gamma' \\ \lambda'_h \\ \delta\lambda'_\gamma \end{bmatrix} = \begin{bmatrix} 0 & V_0 & 0 & 0 \\ K_1 & 0 & 0 & K_2 \\ K_3 & 0 & 0 & -K_1 \\ 0 & K_4 & -V_0 & 0 \end{bmatrix} \begin{bmatrix} \delta h \\ \gamma \\ \lambda \\ \delta\lambda_\gamma \end{bmatrix} \quad (55)$$

where

$$K_1 = [V^2 r^2 - (\beta V^2 + \bar{\mu})r + 2\beta\bar{\mu}] / \beta V r^3 - 2\bar{\mu}^2 / V^3 r^4 - C_L^* S \bar{\mu} M \rho / m V r^2 \quad (56)$$

$$K_2 = -C_L^* S \rho / 2m C_D^* V \quad (57)$$

$$K_3 = -\partial^2 H_{BL} / \partial h^2 \leq 0 \quad (58)$$

$$K_4 = C_D^* S \rho V^3 (1 + 2M^2) / 2m \quad (59)$$

The expressions in (56-59) are evaluated at $h = h_0$, and β is the scale height in an exponential atmospheric model. The term in (58) is complicated to express analytically, but can easily be evaluated numerically taking into account the fact that both H_{BL} and $\partial H_{BL} / \partial h$ evaluated at $h = h_0$ is zero.

The eigenvalues of (55) are arranged symmetrically about the imaginary axis, and occur in complex conjugate pairs. In order to suppress the

instability in the boundary layer response, the state vector in (55) is expressed as

$$x = k_1 \vec{a} + k_2 \vec{b} \quad (60)$$

where $x^T = [\delta h, \gamma, \lambda_h, \delta \lambda_\gamma]$, and \vec{a}, \vec{b} are the real and imaginary parts of the eigenvectors associated with the stable eigenvalues. Knowing δh and γ , it is a simple exercise to solve for k_1, k_2, λ_h and $\delta \lambda_\gamma$. Then L_2^* in (47) can be evaluated for

$$\lambda_\gamma = \bar{\lambda}_\gamma + \delta \lambda_\gamma \quad (61)$$

Equations (46,47) and (61) thus constitute a second feedback guidance law, which we term the "SP2" Solution.

Modeling Energy Rate Dynamics

If energy rate is modeled in the dynamics, the reduced model becomes a two-state problem, and the performance index is modified to minimize $-E(t_f)$. The Hamiltonian in this case is

$$H_0 = \lambda_\psi \dot{\psi} + \lambda_E \dot{E} = 0, \quad \lambda_E(t_f) = -1 \quad (62)$$

This gives rise to a two-point boundary value problem in the reduced solution. However, an approximate integration of λ_E is possible in this case, based on the known properties of the optimal solution. Using (62), it is easy to demonstrate that

$$d\lambda_E/dt = -\partial H_0/\partial E \approx \lambda_E C_D \text{Sp}^2(1+\lambda^2)/2m \quad (63)$$

Thus,

$$d\lambda_E/d\psi = (2C_D^*(1+\lambda^2)\cos\gamma/C_L^*\lambda\sin\mu)\lambda_E \approx (2C_D^*/C_L^*)\lambda_E \quad (64)$$

where the approximations $\lambda \approx 1$, $\mu \approx \pi/2$, $\gamma \approx 0$ have been employed. Integration of (64) results in

$$\lambda_E(\psi) \approx -\exp\{-2C_D^*(\psi_f - \psi)/C_L^*\} \quad (65)$$

Comparing the Hamiltonian expressions in (34) and (62), it can be seen that modeling E as constant in the dynamics amounts to the approximation $\lambda_E = -1$. Equation (65) represents an improvement, but the approximation $\lambda_E = -1$ is apparently accurate for high L/D vehicles. So far as its effect on the reduced solution, (37-41) remain the same. The reduced costate solutions become:

$$\lambda_\psi^0 = -\lambda_E C_D^* V_o^2 (1 + M_o^2)^{1/2} / C_L^* \quad (66)$$

$$\lambda_h^0 = 0, \quad \lambda_\gamma^0 = \lambda_E C_D^* V_o^2 M_o / C_L^* \quad (67)$$

Note that the ψ and γ costate solutions are now simply multiplied by λ_E . The boundary layer solution for L_1^* in (46) remains the same, but (47) becomes

$$L_2^* = -(C_L^*/C_D^* V^2) \lambda_\gamma / \lambda_E \quad (68)$$

Thus the SP1 control solution, which uses $\lambda_\gamma = \lambda_\gamma^0$ remains unchanged when E is modeled in the dynamics, since λ_E is canceled when λ_γ^0 from (67) is substituted in (68). The SP2 solution, on the other hand, is affected in that several of the matrix elements in (55) are changed. In particular, K_2 and K_4 are divided by λ_E and H_{BL} used in the computation K_3 becomes

$$H_{BL} = \lambda_\psi \dot{\psi} + \lambda_h V \sin\gamma + \lambda_\gamma \dot{\gamma} + \lambda_E \dot{E} \quad (69)$$

We will refer to the control solution obtained with these modifications as the "SP3" Solution.

3.2 Numerical Results

A numerical study was performed to evaluate the performance of the three

guidance laws derived in the preceding section. The parameter values, chosen to approximate the vehicle studied in [5], are as follows:

$$C_{D_0} = .032, \quad S = 125.8 \text{ ft}^2, \quad K = 1.4, \quad m = 331.5 \text{ slugs}$$

The initial conditions were chosen to match the 40° heading change maneuver of [5], where the sensible atmosphere was defined to begin at an altitude of 200,000 ft. The corresponding entry velocity and flight path angles are $V(0) = 25,945 \text{ ft/s}$ and $\gamma(0) = -.148^\circ$. A simple exponential atmospheric model was defined using the standard atmospheric data for air density at altitudes of 10^5 and 2×10^5 feet. All of the comparisons are for a 40° heading change.

We first illustrate the validity of the singular perturbation formulation by comparison of the reduced solution altitude profile obtained from the use of (39), with the optimal solution for the 40° plane change problem. The optimal solution was calculated using a multiple shooting method described in [17]. Figure 1 illustrates this comparison. The optimal solution altitude profile satisfies a terminal constraint that $h(t_f) = h(0)$, needed for a typical AOTV orbit plane change. It can be seen that the reduced solution altitude profile closely follows the optimal altitude profile, with the exception of satisfying the initial and final values of altitude, which are lost in the reduced problem formulation (altitude is a control like variable). Clearly, the reduced solution can be used for the initial phase of an AOTV plane change maneuver, but a large terminal boundary layer correction is needed for the exit phase. This aspect will be addressed in Section 4 of this report.

We next consider the performance of the guided solutions for the reentry problem. Figure 2 compares the reduced solution altitude profile obtained from (39) with the SP1 and SP3 guided solution profiles, which on this scale are identical. A similar comparison is given for the SP2 guided solution in Fig. 3. Note that the reduced solution provides a reasonable altitude profile except at high energies near the initial time. However, this region of the solution is of little interest since the air density is negligibly small. In any case, it is not physically possible to follow this profile (recall that h is used as a control variable in the reduced solution). Thus, it was decided to maintain $\lambda = 1$ and $\lambda \cos \mu = -M$ ($\dot{\gamma} = 0$) until $h_0(E)$ falls below the current altitude.

In order to evaluate the optimality of these solutions, an optimal solution was numerically computed using the four-state model in (8-11) to define the dynamics. The SP1 guided solution was used as an initial guess for the state time histories, and the reduced solutions in (44), (54), and (65) were used as an initial guess for the costate time histories. The solution converged to a relative precision of 10^{-12} in eight iterations. The value of the Hamiltonian was constant and essentially zero considering the relative precision accuracy required for convergence. This served as an independent check on the accuracy of the solution.

Figure 4 compares the optimal altitude profile with the profiles that result from the three guided solutions. Note that the optimal solution dips slightly more into the atmosphere near the end, and consequently results in slightly decreased flight time. The corresponding control time histories and heading profiles are compared in Figs. 5-7. Note that in Fig. 5, the optimal bank angle at the final time is 90° , which follows from (47) and the fact that $\lambda_Y(t_f) = 0$. In the context of singular perturbation theory, this gives rise to a terminal boundary layer which must be solved backwards in time. Since this was ignored in our analysis, the guided solutions approach the condition in (48) instead. This explains the departure in the altitude profiles of Fig. 4. It is apparent that this effect is a minor one. In any case, the dip in the optimal profile may not be desirable from a practical standpoint.

It may be somewhat surprising at this point that the SP1 and SP3 solutions are nearly identical. However, recall that the SP1 solution is not sensitive to the approximation that E is modeled as constant in the dynamics. The SP3 solution corrects the SP2 solution for this modeling approximation, and results in essentially the same solution as the SP1 solution. This fact also justifies the use of approximation $\lambda_Y = \lambda_Y^0$ in the SP1 solution. Table 1 compares the energy loss for all the solutions, and shows the three guided solutions produce essentially optimal performance. The energy loss for the SP1 and SP3 solutions is indistinguishable from the optimal solution to four significant places, while the energy loss for the SP2 solution is .06% greater.

SECTION 4

AEROASSISTED ORBIT TRANSFER

The preceding section has demonstrated that singular perturbation theory can be used as an effective tool in model order reduction for the problem of hypervelocity heading change within the atmosphere with minimal energy loss. The extension to aeroassisted orbit transfer with inclination change requires that a constraint be imposed on the terminal altitude to insure that the vehicle exits the atmosphere when the heading change (which approximates the inclination change) is achieved. This introduces a difficult terminal boundary layer problem, which to date we have not been able to solve in closed form, since it requires an analytic integration of the boundary layer equations. In [5-9] this same problem arises, but in a different context. In these studies, the states and co-states associated with a four-state model are analytically integrated with the assumption that Loh's term, $M(h,V)$, is constant or piecewise constant over the trajectory. While this is true for a large portion of the maneuver, M undergoes a large variation near the end. Consequently, the guidance algorithms resulting from these studies require large angles of attack near the end of the maneuver to compensate for this variation. This drawback was subsequently removed in [10], however, the resulting guidance algorithm requires that a complex quadrature be performed at each guidance interval. Moreover, this approach is not readily extended to the case where heating rate is constrained.

The essential problem in all these approaches lies in the fact that air density decreases exponentially as altitude increases, and corrections to satisfy terminal constraints must be accurately predicted while the vehicle is at lower altitudes.

In this section, the simplest guidance algorithm presented in Section 3 is used for the initial portion of the maneuver, and a predictor/corrector type algorithm is presented for the terminal maneuver. The predictor/corrector algorithm relies on bank angle control alone, and thus avoids the problem of large angle of attack. The form of the guidance algorithm was chosen to closely approximate the known properties of the optimal solution, while permitting an accurate integration of the equations of motion. The predictor/corrector algorithm provides the information needed

to both initiate the terminal maneuver, and to guide the vehicle in closed loop fashion. The availability of a closed loop guidance algorithm will be of paramount importance in future studies addressing the effect of atmospheric anomalies, and of course, for real time implementation. Comparisons are made to numerically optimized trajectories for a range of orbit plane angles to demonstrate the near optimality of the complete guidance algorithm.

4.1 Guidance During the Reentry Phase

Guidance during the reentry phase is based on the zero order reduced and boundary layer solution referred to as the SP1 solution in Section 3. This consists of first calculating the reduced solution in (39), and then calculating the horizontal and vertical components of the normalized lift vector using (46,47), with $\lambda_Y = \lambda_Y^0$ as given by (48).

4.2 Guidance During the Exit Phase

The reentry phase guidance algorithm does not satisfy the terminal constraint on h , which was lost in the reduced formulation. The terminal boundary layer necessary conditions are identical in form to those for the initial boundary layer. However, the solution asymptotically approaches the reduced solution backwards in time, starting from the terminal constraint on altitude. In addition, the change in ψ during the terminal maneuver must be accounted for to insure that both terminal constraints are met simultaneously. This requires an analytical integration of the state and costates. To circumvent this problem, a predictor/corrector guidance law was developed based on the known properties of the optimal solution: $\lambda^* \approx 1.0$, $\mu^* \approx \pi/2$.

To simplify the problem of integrating the forward motion, it is assumed that the nominal exit maneuver consists of two regions. In the first, a constant (negative) bank angle perturbation is used to increase the flight path angle. This is followed by a second region in which γ is influenced only by gravity. A bank angle correction is computed throughout the maneuver

based on the predicted heading error at the final altitude. Constraints are enforced to insure continuity at the junction of the two regions, and satisfaction of the terminal constraint on altitude. The maneuver is depicted in Fig. 8.

During terminal guidance, we maintain $\lambda = 1.0$, and modulate the bank angle according to the following equations:

$$\mu = \mu_0 - \delta\mu_0 + \delta\mu = \mu + \delta\mu \quad (70)$$

where in Region 1:

$$\mu_0 = \cos^{-1}(-M), \quad \delta\mu_0 = \text{const.} > 0 \quad (71)$$

and in Region 2:

$$\mu_0 = 90^\circ, \quad \delta\mu_0 = 0 \quad (72)$$

The nominal trajectory can be analytically predicted for $\delta\mu=0$, and using the approximations:

$$\cos \mu \approx -M + \delta\mu_0 \sin \mu_0, \quad \sin \gamma \approx \gamma \quad (73)$$

the details of which can be found in [18]. The predicted heading change ($\Delta\psi_p$) for the exit maneuver is calculated at each integration step along the trajectory, and is used to both initiate the maneuver (when $\Delta\psi_p = \psi_{go}$), and to track the terminal constraint using a simple proportional control law,

$$\delta\mu = k(\psi_{go} - \Delta\psi_p) \quad (74)$$

Region 2 guidance is initiated when the present altitude satisfies the continuity constraint at the junction of the two regions.

4.3 Numerical Results

A numerical study was performed to evaluate the performance of the sub-optimal guidance algorithm described in the preceding section, using the same vehicle data as presented in [6] and in Section 3. Fig's 9 and 10 illustrate the guided altitude profiles and the corresponding bank angle profiles obtained for heading changes up to 40° , in increments of 10° . The λ profiles are very close to 1.0 throughout for all the maneuvers, and are not

illustrated. These results were generated for $\delta\mu_0 = 25^\circ$, $k = 50$, however it was found that the general character of the solutions did not change as these guidance parameters were varied. Note from Fig. 10 that, following the initial perturbation, bank angle continues to decrease in Region 1. This is due to the variation in M that takes place as the altitude departs from the reduced solution profile. After completing Region 1, the bank angle remains very close to 90° , or in other words, $\delta\mu$ in (24) is very close to zero, indicating the accuracy of the prediction algorithm.

In order to evaluate the optimality of the guidance algorithm, optimal solutions were obtained numerically using the multiple shooting algorithm [17]. Fig's. 11 and 12 illustrate the optimal altitude and bank angle profiles. The most remarkable characteristic in these solutions is that the final time is nearly independent of the final heading. Also note that the final bank angle is always 90° , which is required by the necessary conditions. The corresponding λ profiles are shown in Fig. 13, which verifies that the optimal solution lies close to $\lambda = 1$. The flight path angle histories for all the cases in Fig. 9 and Fig. 12 are quite small, and close to zero at the final time.

Despite the fact that the final times are considerably different, the guided solution performance is not far from optimal. Table 2 illustrates the near optimality by comparing the energy loss of the guided solutions with that of the optimal solutions.

SECTION 5

CONSTRAINED AEROGLIDE

The constrained aeroglide problem is treated in this section. This is essentially the same problem addressed in Section 4 with the addition of a heating rate constraint, which amounts to a first order state variable inequality constraint.

5.1 Problem Formulation

For this problem it is necessary to consider the system of equations in (2-6), since the approximation that $\phi = 0$ is no longer valid. In this case, θ remains an ignorable coordinate, and (7) is used to define the change in inclination angle. It was also necessary to initiate the maneuver at a much higher altitude, since the starting condition for the results in Section 4 has a fairly high value of heating rate. Only numerically optimized solutions were considered, using the same multiple shooting method that was employed for the unconstrained solutions. First the touch point solution was considered, and the range of maximum allowable heating rate over which this solution applies was obtained for the same vehicle dynamics considered in Section 4. Then, the constrained arc solution was attempted for lower values of the heating rate limit. However, only a narrow range of solutions were found for this case. Unfortunately, all of these solutions violate the practical limits for heating rate. Hence, the optimal aeroglide problem remains an open research issue. It may be that very complex behavior results for lower values of heating rate limit, such as multiple touch point solutions combined with portions of a constrained arc.

The expression for heating rate employed in this study was:

$$dQ/dt = 17600[p/p_s]^{1/2}[V/V_s]^{3.15} \quad (\text{BTU/sec/ft}^2) \quad (75)$$

5.2 Numerical Results

The vehicle characteristics are the same as those given in Section 3.3. The initial and terminal condition data are as follows:

$$h(0) = h(t_f) = 365,000 \text{ ft}, \quad V(0) = 25,746 \text{ ft/s}, \quad \gamma(0) = 0.55^\circ$$

$$i(t_f) = 18^\circ$$

The initial h , V and γ correspond to the same deorbit impulse employed in Sections 3 and 4.

Figures 14-16 illustrate the h , V and i profiles for the unconstrained solution and for the touch point solution corresponding to a maximum heating rate of 600 BTU/sec/ft^2 . As the heating rate limit is decreased, the minimum altitude and flight time increase. Figures 17 and 18 show the corresponding control time histories. For the touch point solution, there is a slight jump in the normalized lift coefficient at the touch point. However, this is likely due to numerical inaccuracy in satisfying the touch point conditions. The bank angle history is continuous. Figures 19 and 20 illustrate the jumps that occur in the λ_h and λ_V at the touch point. All other costates are continuous. All of the state and costate histories can be found in [18]. Figure 21 compares the heating rate profiles. The peak heating rate for the unconstrained case was $729.3 \text{ BTU/sec/ft}^2$. In comparing these results it was found that the increase in energy loss due to the heating rate limit imposed was negligible. However lower heating rate limits will likely result in much greater energy loss.

Attempts to decrease the heating rate limit below 600 BTU/sec/ft^2 resulted in convergence failure. This failure was abruptly encountered at a heating rate limit of $599.3 \text{ BTU/sec/ft}^2$. Thus we suspect that either a conjugate point is encountered, or the nature of the optimal solution changes to either a constrained arc case or a multiple touch point case. The constrained arc case was investigated, and after many attempts (including reformulation in nondimensional variables) we were not able to obtain a converged solution.

SECTION 6

CONCLUSIONS AND RECOMMENDATIONS

The application of singular perturbation methods to optimal control problems related to aeroassisted orbit transfer vehicles has been investigated in this study. Two closely related problem formulations were addressed: optimal reentry of a hypersonic gliding vehicle, and optimal orbit plane change with aeroglide. In addition, an attempt was made to obtain numerical solutions for optimal aeroglide orbit plane change subject to a maximum heating rate constraint.

6.1 Conclusions

The major conclusions resulting from this research effort are as follows:

- (1) Singular perturbation theory using energy state approximations can be used to reduce the model order to a single state equation, and a closed form solution for the reduced problem can be readily obtained. The solution for the reduced problem reasonably approximates the full order optimal solution, except near the initial and final conditions. By non-dimensionalizing the equations of motion a singular perturbation expansion parameter can be identified that depends on vehicle parameters and the required heading change.
- (2) For the reentry problem, three guidance algorithms were derived, all of which are nearly optimal in terms of minimizing the energy loss for the maneuver. No terminal boundary layer correction was required for this problem formulation.
- (3) A constraint on terminal altitude, required for the noncoplanar orbit transfer problem, results in a difficult boundary layer problem for which we were not able to obtain a tractable analytic solution. However, the optimal terminal maneuver was approximated

using a sub-optimal predictor/corrector guidance law. In general, optimization of the terminal maneuver (to satisfy terminal constraints) is not as critical as optimizing the initial (reentry) portion of the maneuver.

- (4) The problem of optimal orbit plane change subject to a heating rate constraint results in a touch point extremal solution for a high (but narrow) range of heating rate limit. These trajectories and the corresponding control histories are similar to the unconstrained solution, with negligible increase in energy loss. This will not be true for lower values of the heating rate limit, where the constrained trajectory may ride the constraint boundary and/or contain multiple touch points. Unfortunately, the multiple shooting method could not be successfully used to find extremal solutions corresponding to the first order necessary conditions associated with this problem.

6.2 Recommendations

Based on the results of this research effort, the recommendations for further work along this line are:

- (1) The numerical study of optimal aeroassisted orbit transfer with aeroglide, subject to a heating rate constraint, should be completed over a more practical range of heating rate limit. Along this line, alternative formulations of the necessary conditions, such as the transformation method in [19], should be explored. Another approach is to use a parameter optimization based method such as that employed in OTIS [20]. In this case, the constraint would be enforced indirectly through a penalty function approach. The resulting profiles are of interest for comparison to aerocruise solutions [12], and for further developing near optimal guidance algorithms based on singular perturbation theory.
- (2) Further research is needed to develop methods of solving the terminal boundary layer problem associated with terminal

constraints. One such alternative, investigated in this study [18] (but not reported here), is a formulation in which the terminal altitude constraint was satisfied as a part of the reduced solution. This avoids the terminal boundary layer problem altogether.

- (3) Parametric studies of the effect of initial and final orbit altitudes on the optimal orbit plane change maneuver should be conducted. This includes the possibility of optimizing the deorbit impulse, and including the use of multiple impulsive maneuvers for performing a part of the orbit inclination change outside the atmosphere.
- (4) Robustness of the guidance algorithms resulting from this study was not investigated. In particular, the effect of uncertain atmospheric conditions at high altitudes should be evaluated.
- (5) Extensions to problem formulations suitable for aerocapture and orbit plane change for future Mars missions should be explored.

6.3 Publications

The journal and conference publications that resulted from this research effort can be found in [18] and in [22-26].

REFERENCES

1. Bryson, A.E., Desai, M.N., and Hoffman, W.C., "Energy-State Approximation in Performance Optimization of Supersonic Aircraft," *Journal of Aircraft*, Vol. 6, Nov.-Dec. 1968.
2. Calise, A.J., "Singular Perturbation Methods for Variational Problems in Aircraft Flight," *IEEE Trans. on A.C.*, Vol. AC-21, No. 3, June 1976.
3. Calise, A.J., "Extended Energy Management Methods for Flight Performance Optimization," *AIAA Journal*, Vol. 15, No. 3, May-June 1976.
4. Calise, A.J., "Singular Perturbation Techniques for On-Line Optimal Flight-Path Control," *AIAA J. of Guid. and Cont.*, Vol. 4, No. 4, July-Aug. 1981.
5. Mapar, J., "Development and Comparison of Optimal Guidance Laws for Aeroassisted Orbital Transfer," MS Thesis, University of Texas at Austin 1984.
6. Hull, D.G., Giltner, J.M., Speyer, J.L. and Mapar, J., "Minimum Energy-Loss Guidance for Aero-Assisted Orbital Plane Change," *AIAA J. of Guid., Cont., and Dyn.*, Vol. 8, No. 4, July-Aug. 1985.
7. Hull, D.G., "New Analytical Results for AOTV Guidance," *AIAA GN&C Conf.*, Snowmass, CO, Aug. 1985.
8. Hull, D.G., McClendon, J.R., Speyer, J.L., "Aero-assisted Orbital Plane Change Using an Elliptic Drag Polar," *Journal of the Astron. Sciences*, Vol. 36, Nos. 1/2, Jan.-June 1988.
9. Hull, D.G., McClendon, J.R., Speyer, J.L., "Improved Aero-assisted Plane Change Using Successive Approximation," *Journal of the Astron. Sciences*, Vol. 36, Nos. 1/2, Jan.-June, 1988.
10. Speyer, J.L., Crues, E.Z., "An Approximate Atmospheric Guidance Law for Aeroassisted Plane Change Maneuvers," *AIAA GN&C Conf.*, Minneapolis, MN, Aug. 1988.
11. Hull, D.G. Speyer, J.L., "Optimal Reentry and Plane-Change Trajectories," *Journal of Astron. Sciences*, Vol. 30, No. 2, April-June 1982.
12. Mease, K.D., Lee, J.Y., Vinh, N.X., "Orbital Changes During Hypervelocity Aerocruise," *Journal of the Astron. Sciences*, Vol. 36, Nos. 1/2 Jan-June 1988.
13. Lee, J.Y., Hull, D.G., "Maximum Orbit Plane Change with Heat-Transfer-Rate Constraints," *AIAA J. of Guid., Cont. and Dyn.*, to appear.

14. Mease, K.D., "Optimization of Aeroassisted Orbital Transfer: Current Status," Journal of the Astron. Sciences, Vol. 36, Nos. 1/2, Jan.-June 1988.
15. Ardema, M.D., "Linearization of the Boundary Layer Equations of the Minimum Time-To-Climb Problem," J. of Guid. and Cont., Vol. 2, No. 5, Sept.-Oct. 1979.
16. Calise, A.J., "Optimization of Aircraft Altitude and Flight-Path Angle Dynamics," J. of Guid., Cont. and Dyn., Jan.-Feb. 1984.
17. Burlish, R., "The Multiple Shooting Method for Numerical Solution of Nonlinear Boundary Value Problems and Optimal Control Problems (in German), Carl-Cranz-Gesellschaft, Techn., Rep., Heidelberg, 1971.
18. Bae, Gyoung-Hyun, "Optimal Control of Aero-Assisted Orbit Transfer Vehicles, Ph.D. Thesis, Georgia Institute of Technology, December 1988.
19. Jacobson, D.H. and Lele, M.M., "A Transformation Technique for Optimal Control Problems with a State Variable Inequality Constraint," IEEE Trans. on A.C., Vol. AC-14, No. 5, Oct. 1969.
20. Paris, S.W., Hargraves, C.R., "Optimal Trajectories by Implicit Simulation - Vol's. I-IV," AFWAL-TR-88-3057, Flight Dynamics Lab., Air Force Wright Aeronautical Labs., WPAFB, November 1988.
21. Calise, A.J., Bae, G.H., "Singular Perturbation Analysis of AOTV-Related Trajectory Optimization Problems," Progress Report for 1 Sept. - 30 July, July 1987.
22. Calise, A.J., "Singular Perturbation Analysis of the Atmospheric Orbital Plane Change Problem," Journal of the Astron. Sciences, Vol. 36, Nos. 1/2, Jan.-June 1988.
23. Calise, A.J., Bae, G.H., "Optimal Guidance for Aeroassisted Orbit Transfer Vehicles," American Control Conf., Atlanta, Ga., June 1988.
24. Calise, A.J., Bae, G.H., "A Near Optimal Guidance Algorithm for Aeroassisted Orbit Transfer," AIAA Guidance, Navigation and Control Conf., Minneapolis, MN, August 1988.
25. Calise, A.J., Bae, G.H., "Aeroassisted Orbit Transfer with a Heating Rate Constraint," IEEE International Conf. on Cont. and Appl., Jerusalem, Israel, April 1989.
26. Calise, A.J., Bae, G.H., "Optimal Heading Change with Minimum Energy Loss for a Hypersonic Gliding Vehicle," AIAA J. of Guidance Dynamics and Control, to appear.

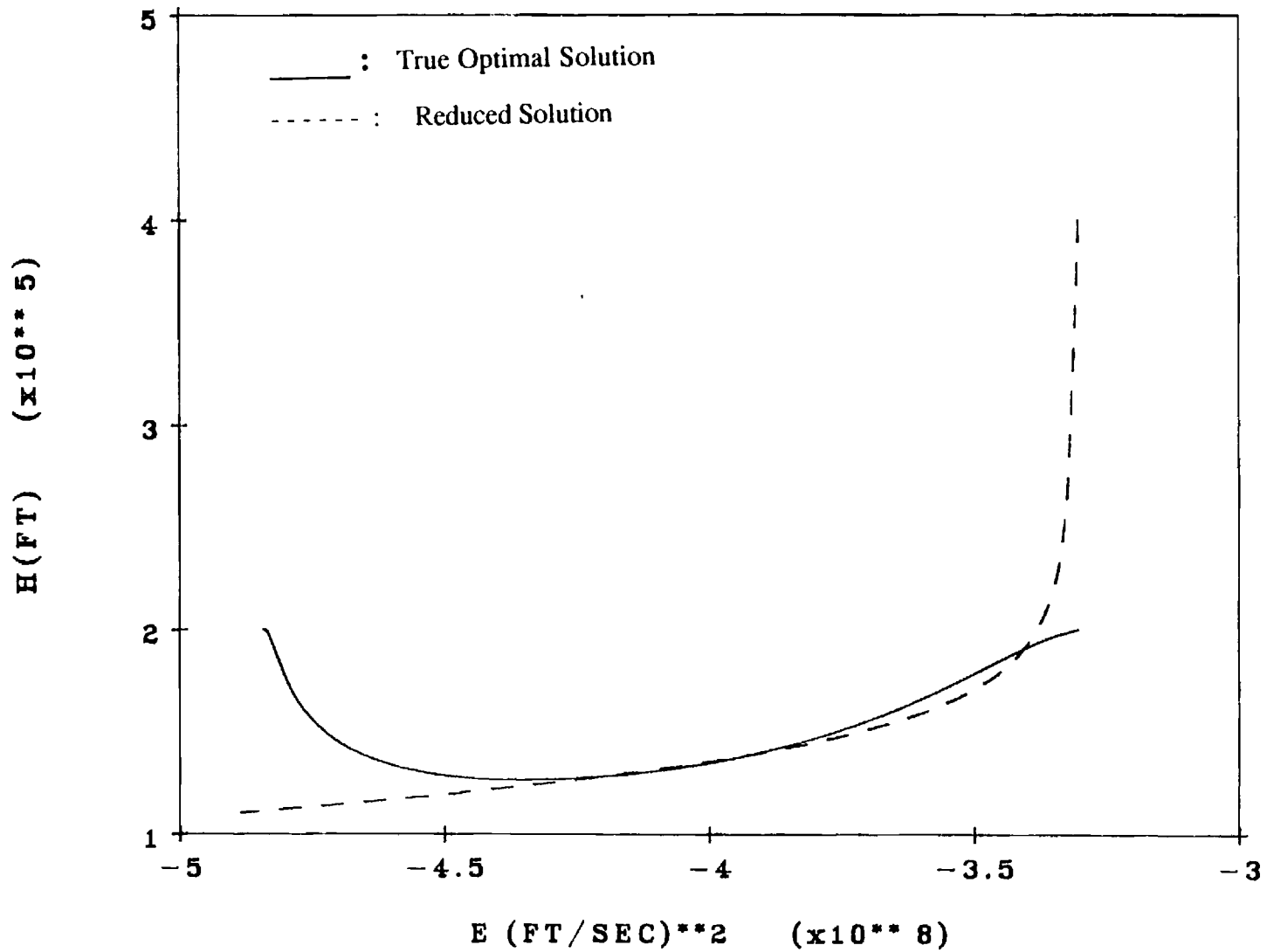


Figure 1. Comparison of the reduced solution altitude profile with an optimal profile for a 40° heading change.

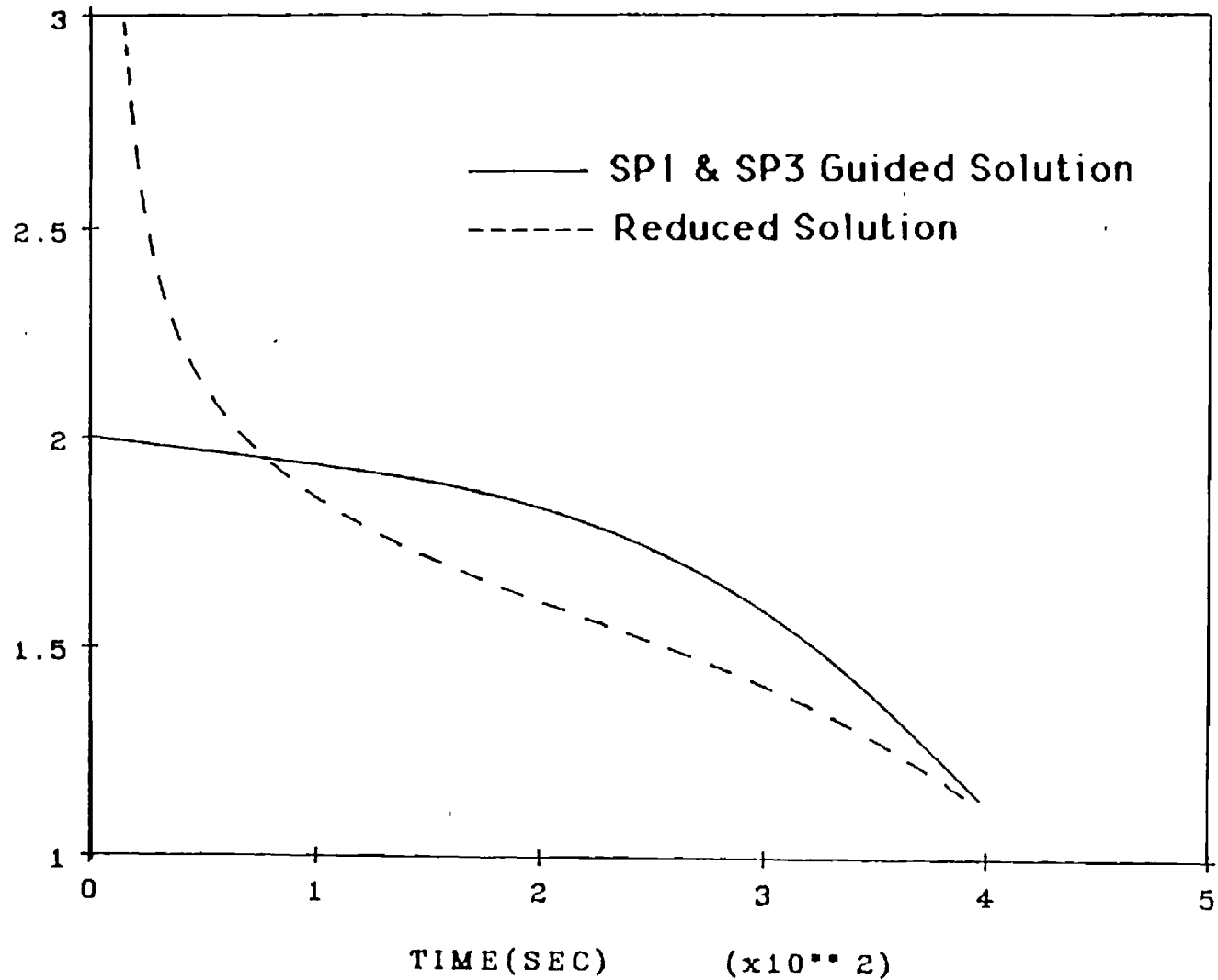


Figure 2. Comparison of the SP1 and SP3 guided altitude profiles with the reduced solution.

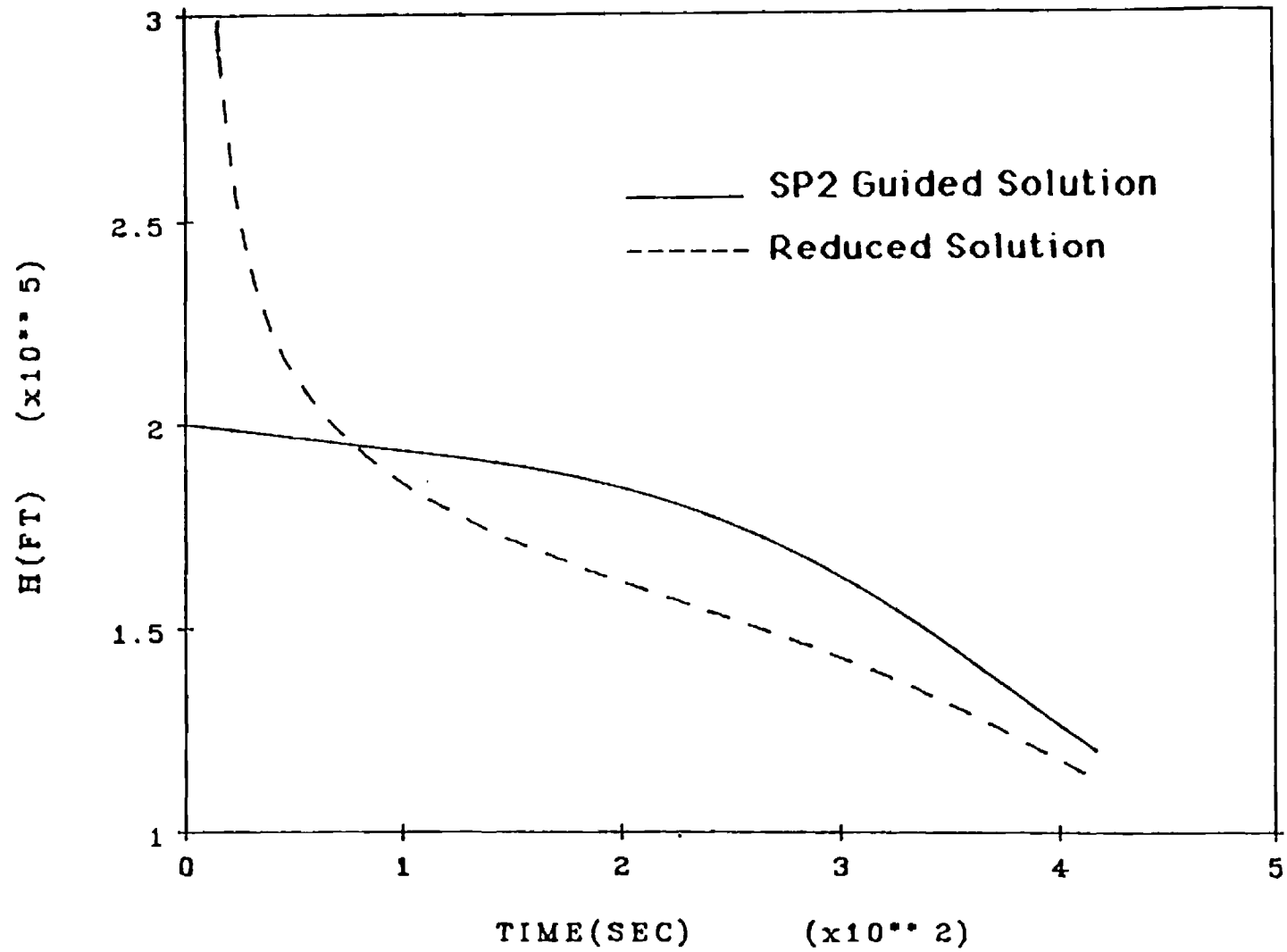


Figure 3. Comparison of the SP2 guided altitude profile with the reduced solution.

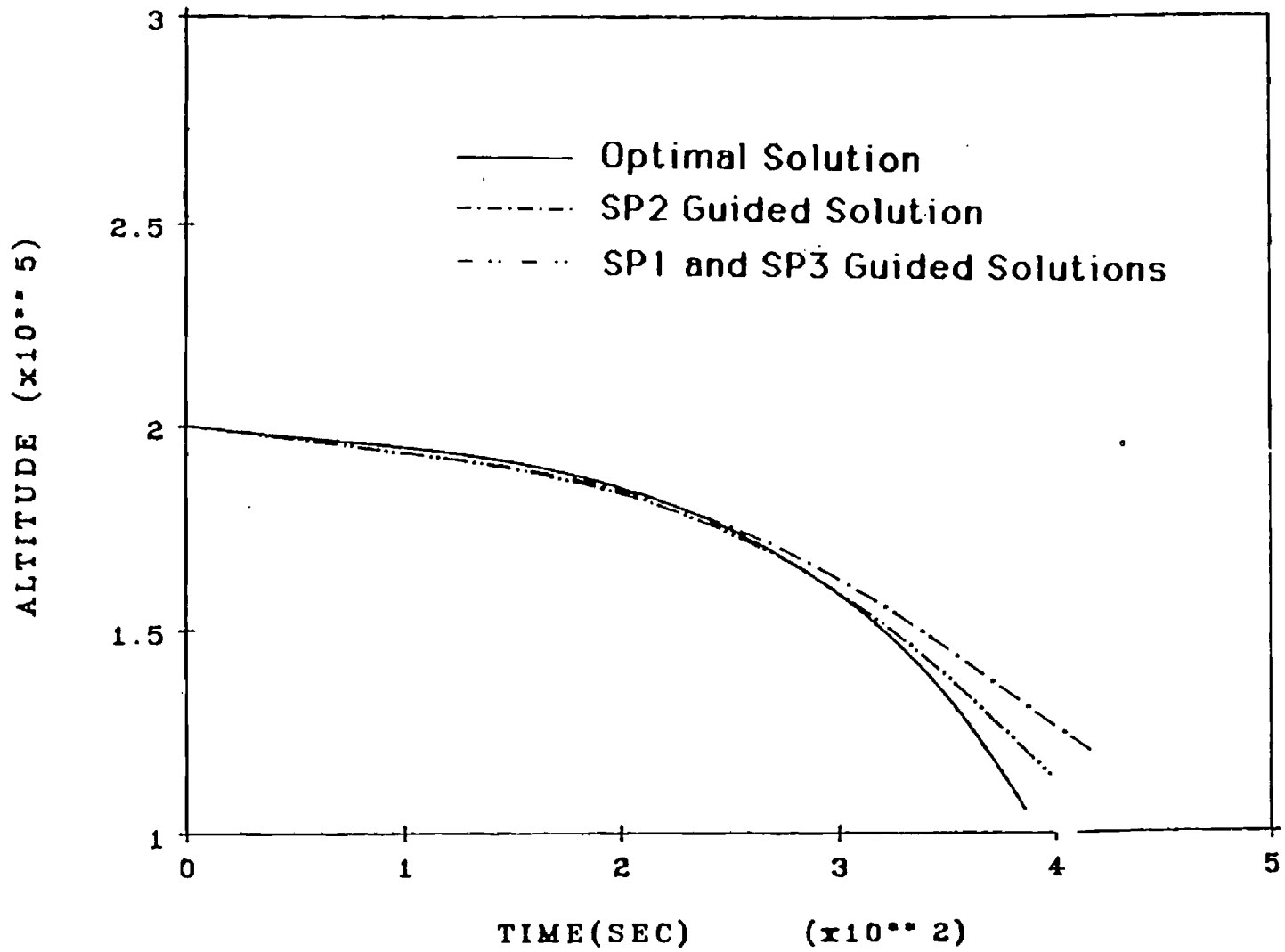


Figure 4. Comparison of the guided altitude profiles with the true optimal solution.

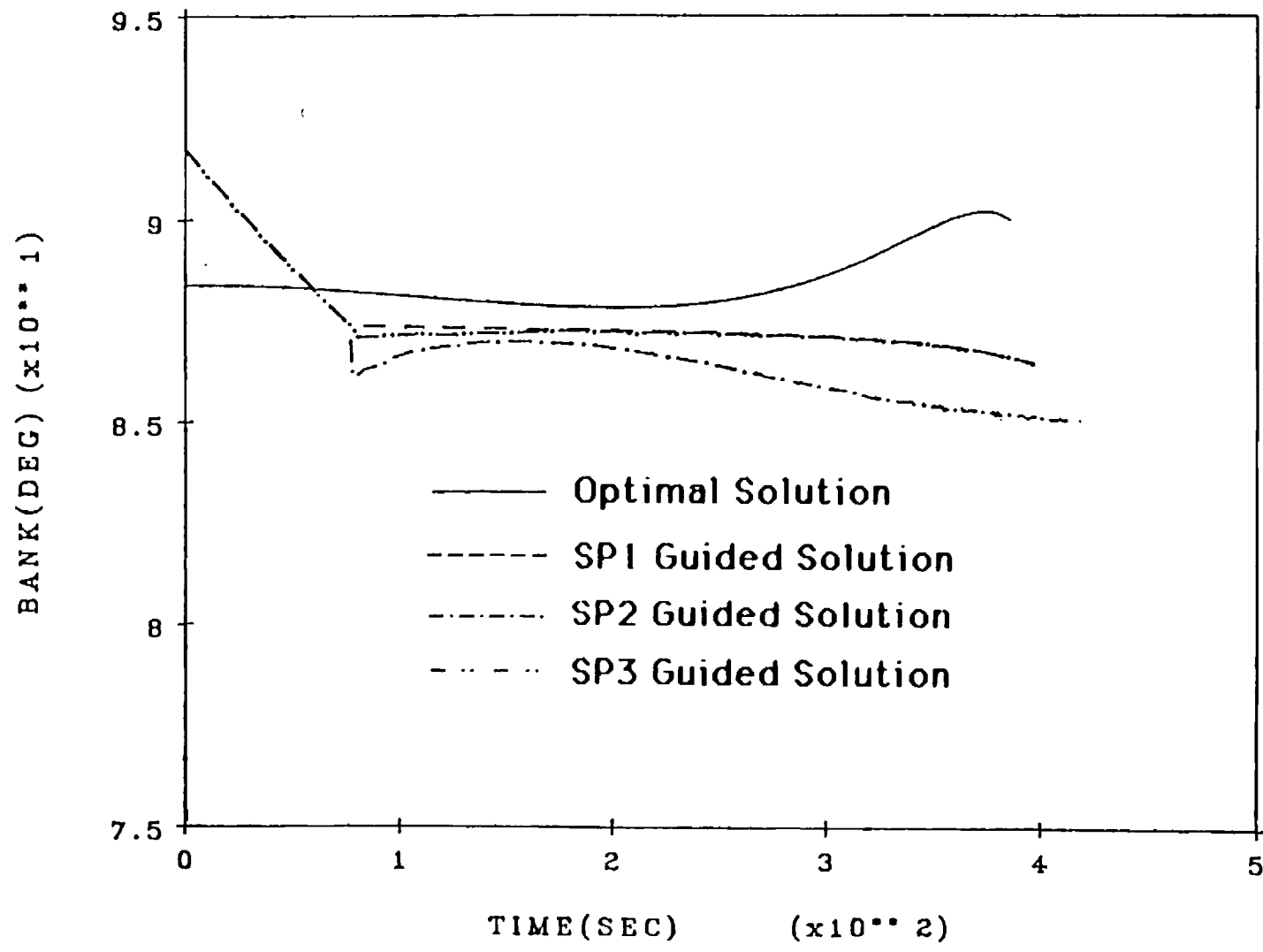


Figure 5. Bank angle profiles.

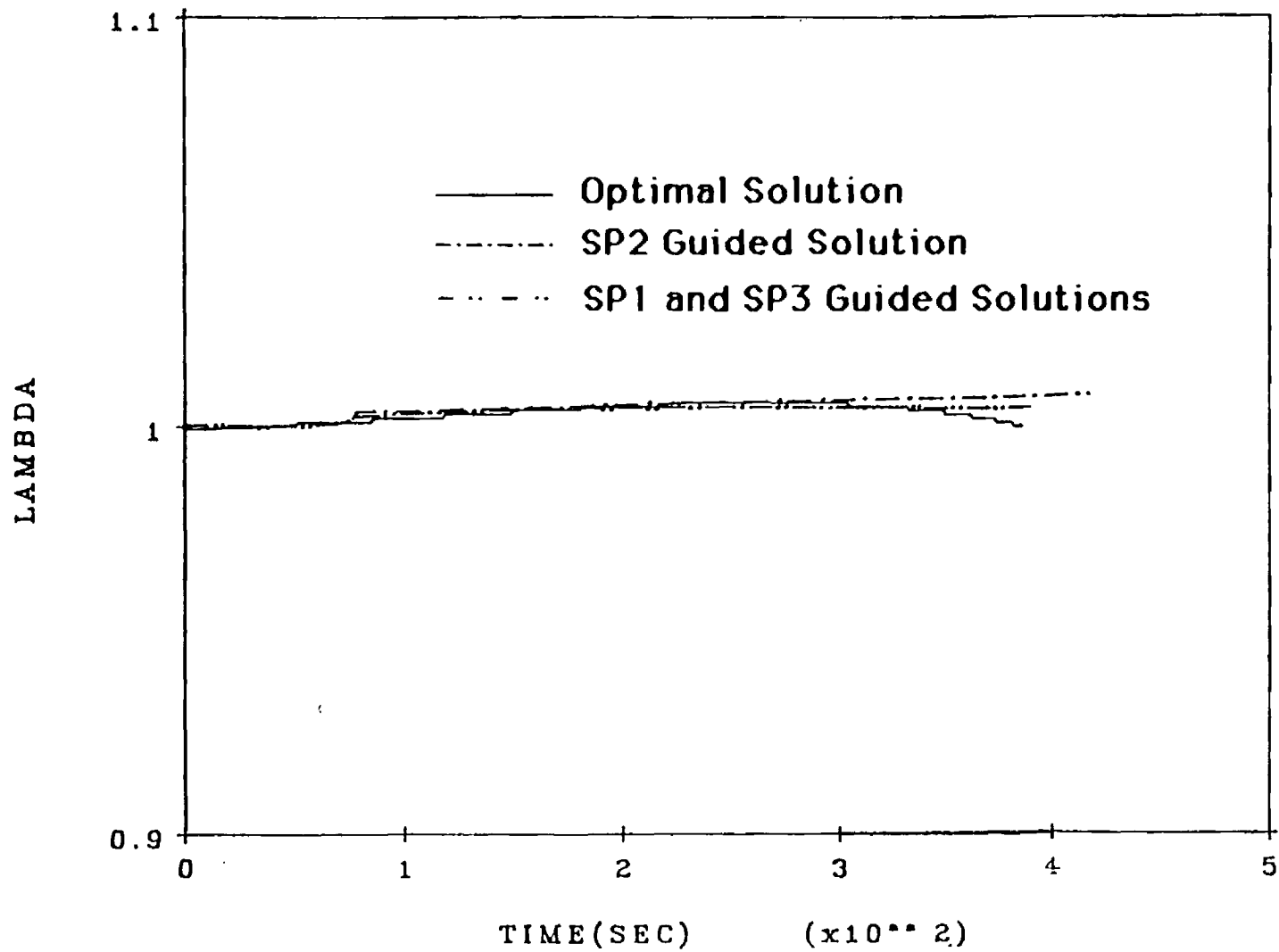


Figure 6. Normalized lift coefficient profiles.

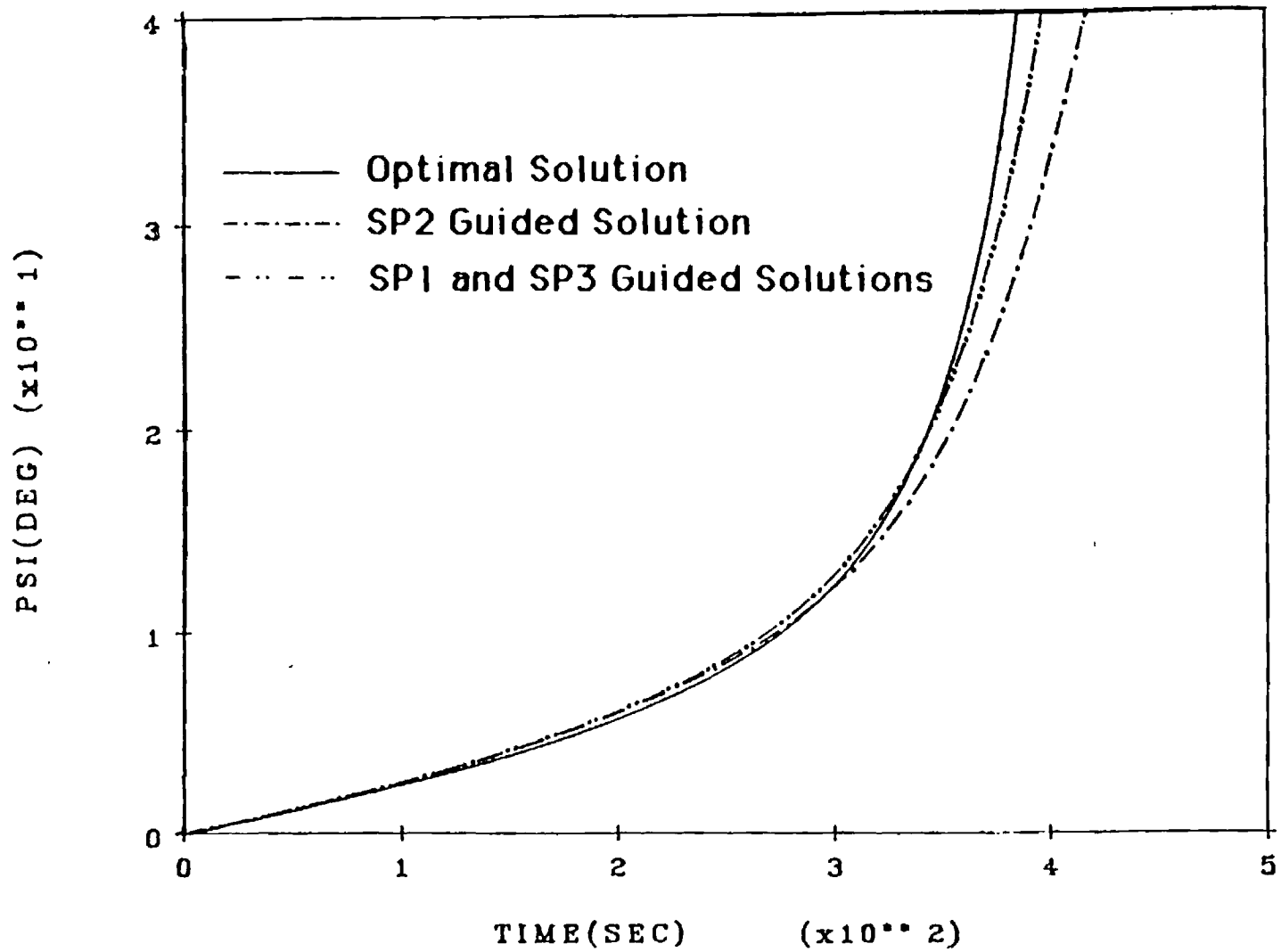


Figure 7. Heading profiles.

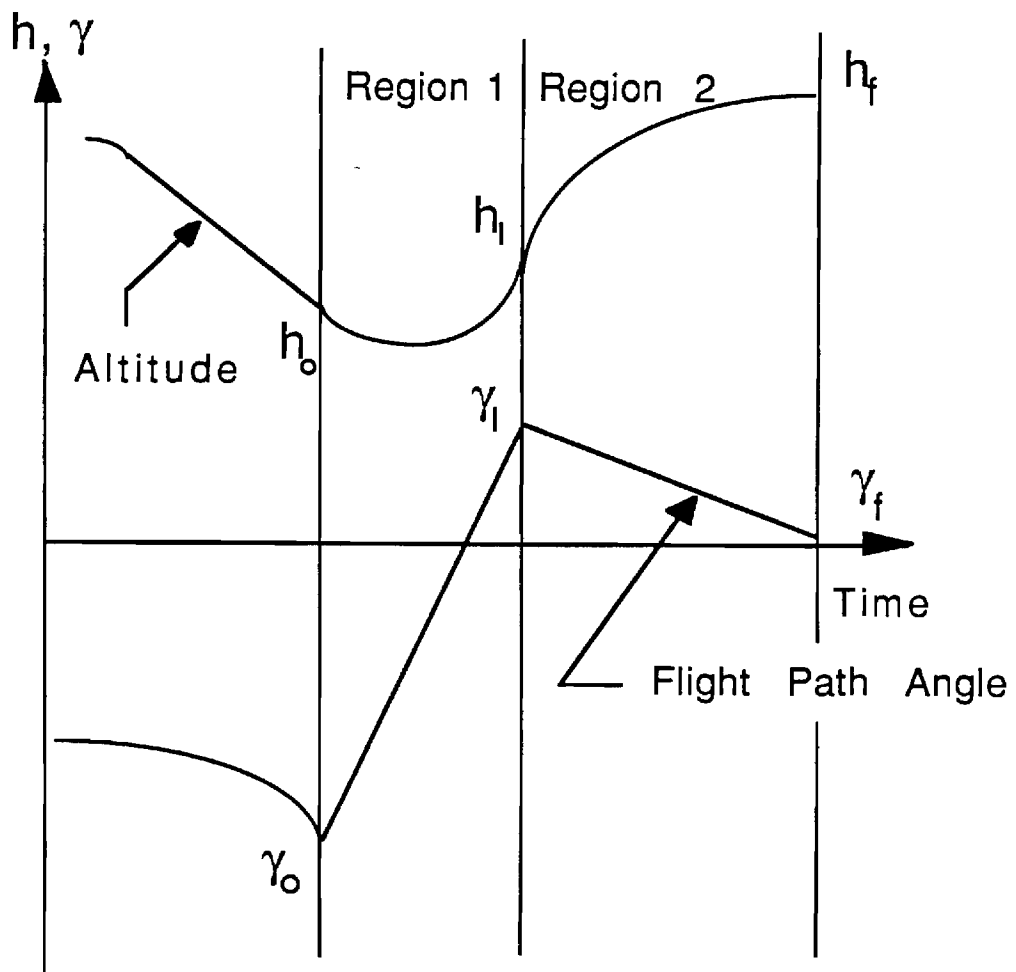


Figure 8. Depiction of the exit phase maneuver.

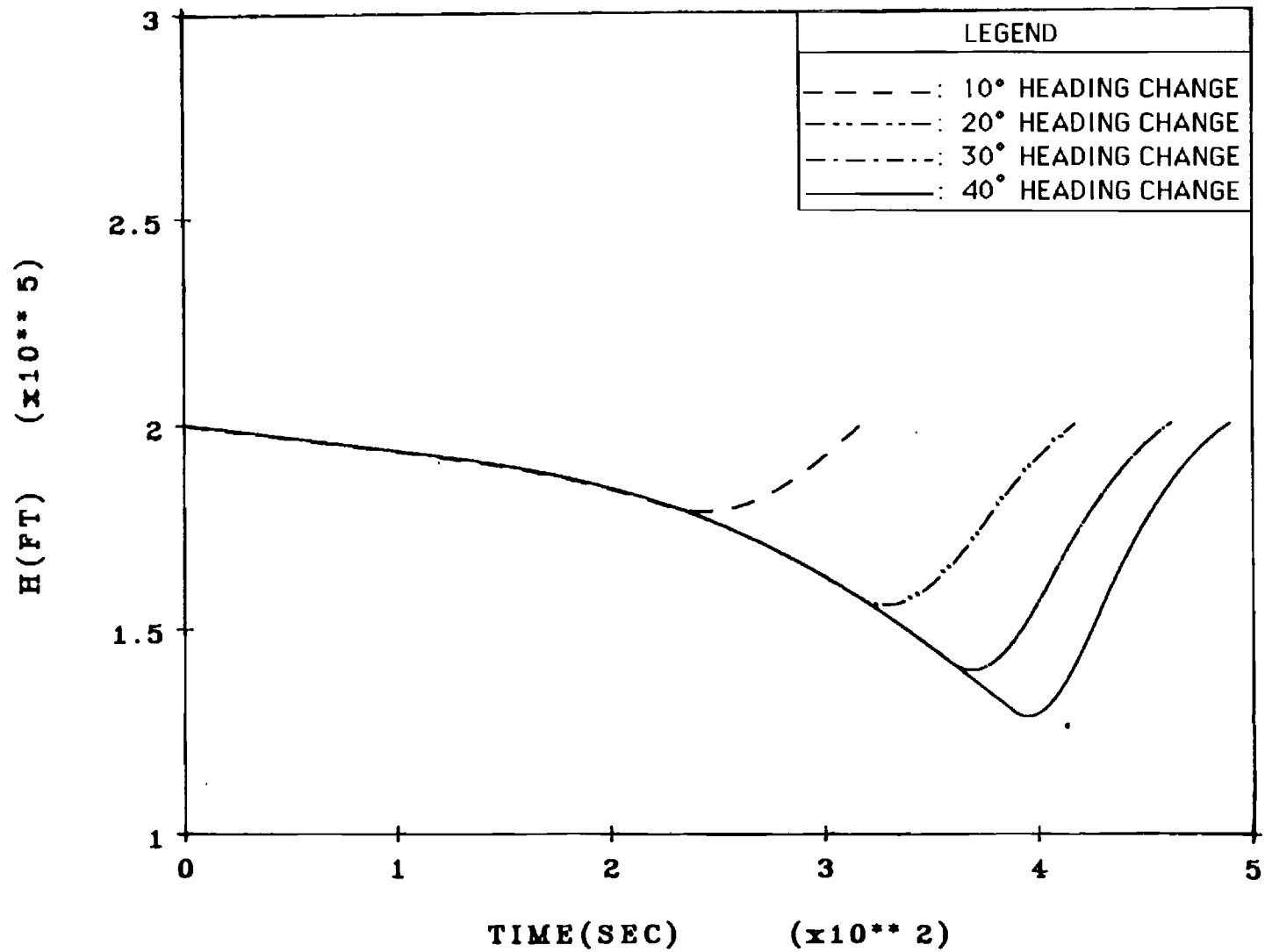


Figure 9. Guided solution altitude profiles.

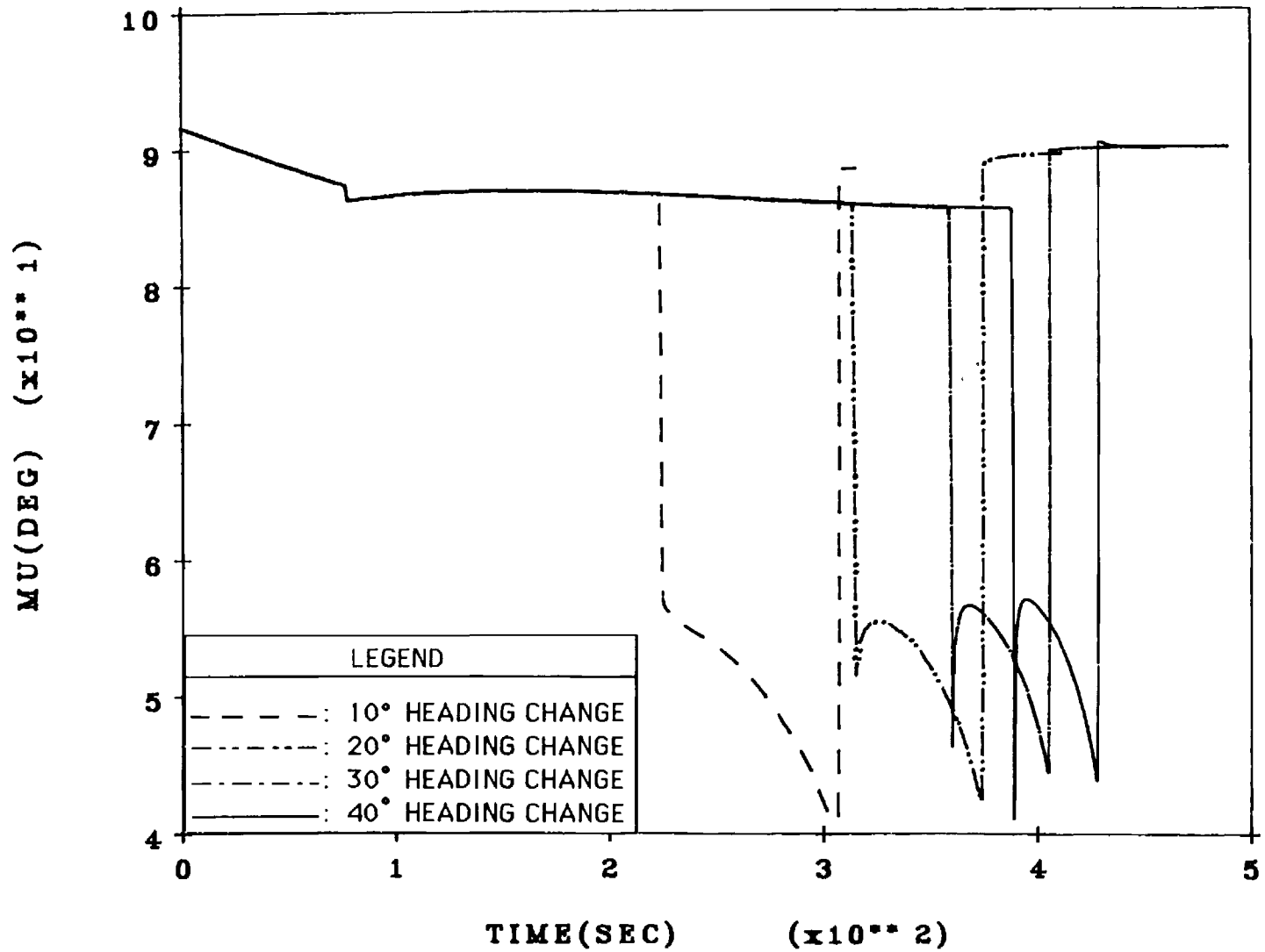


Figure 10. Guided solution bank angle profiles.

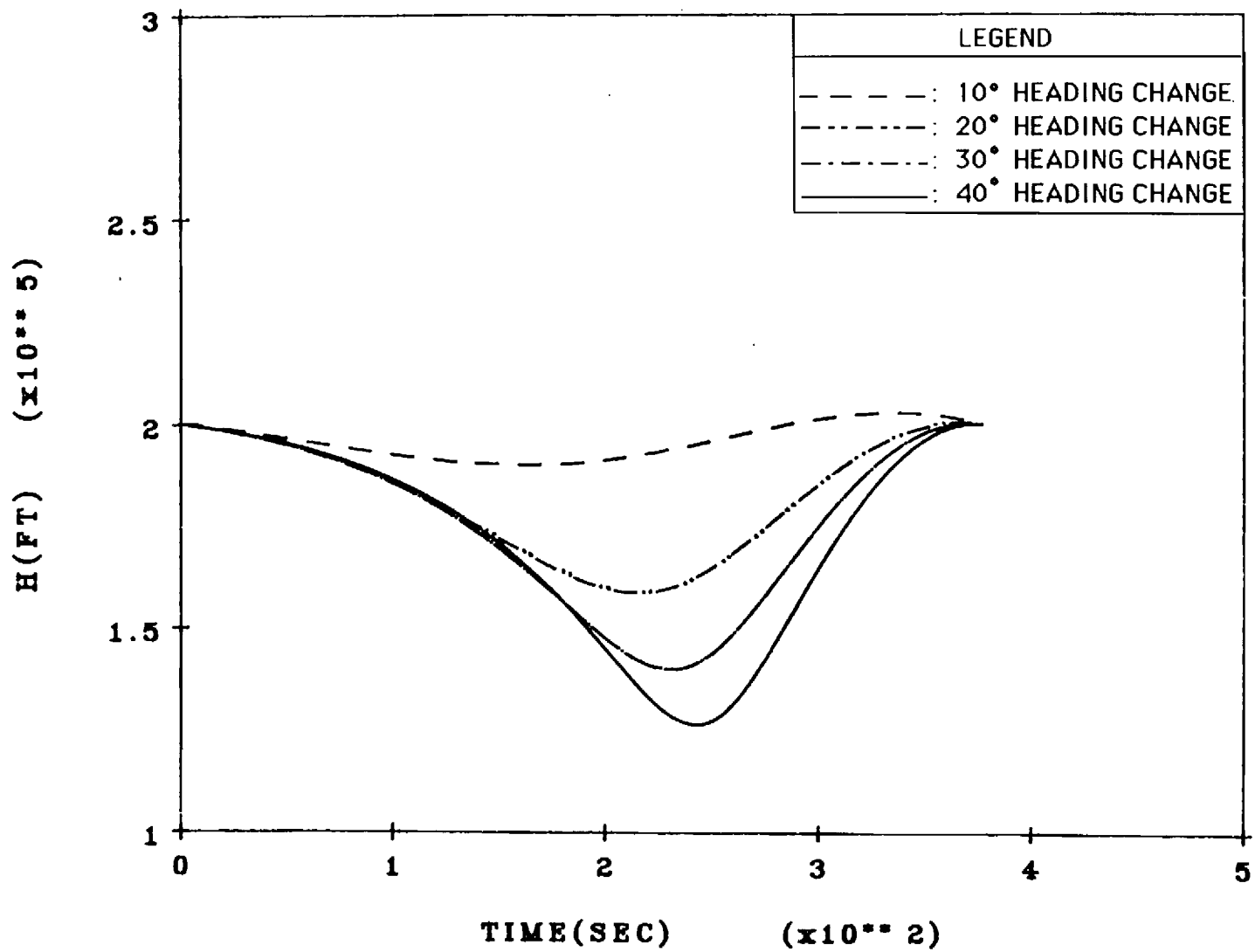


Figure 11. Optimal solution altitude profiles.

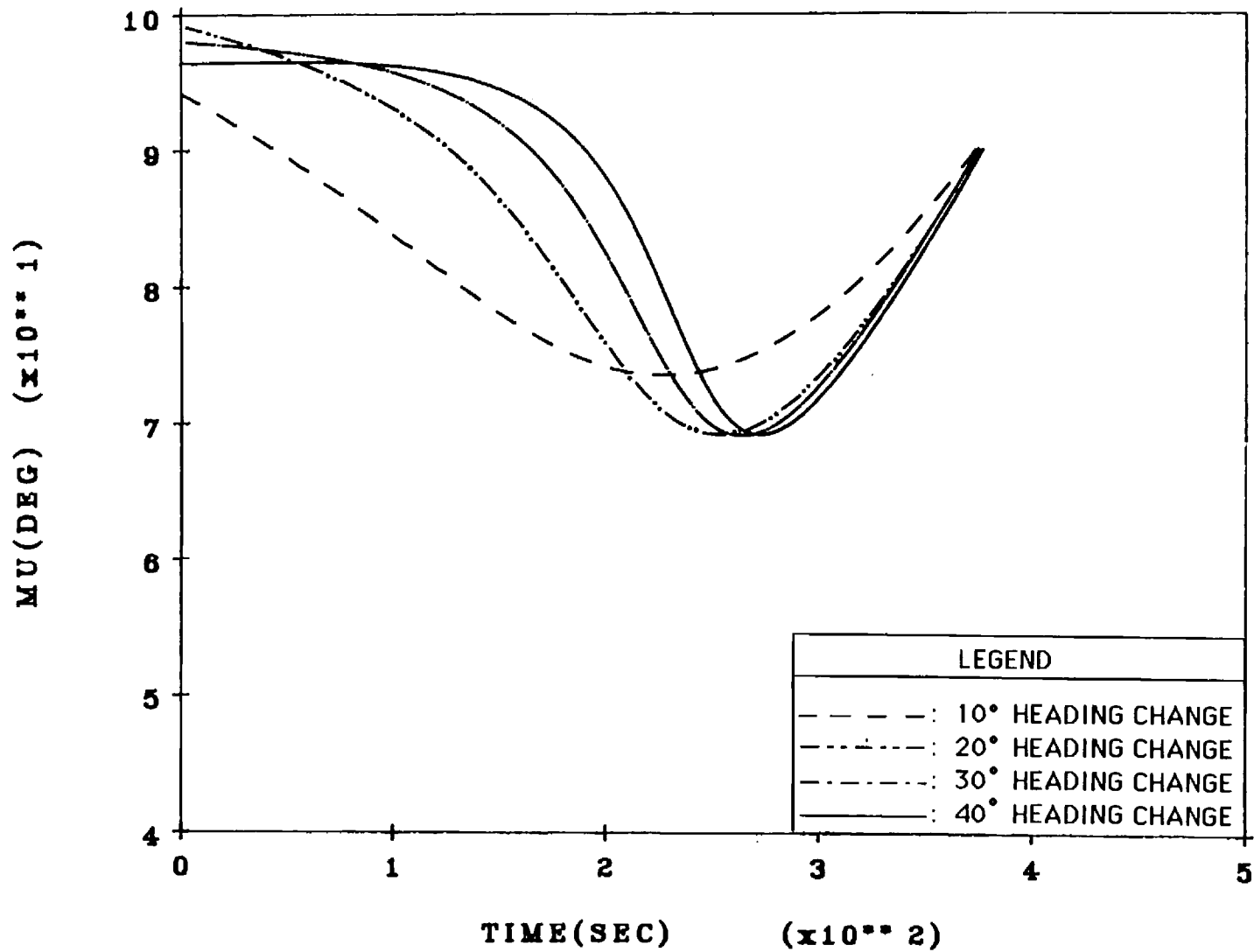


Figure 12. Optimal solution bank angle profiles.

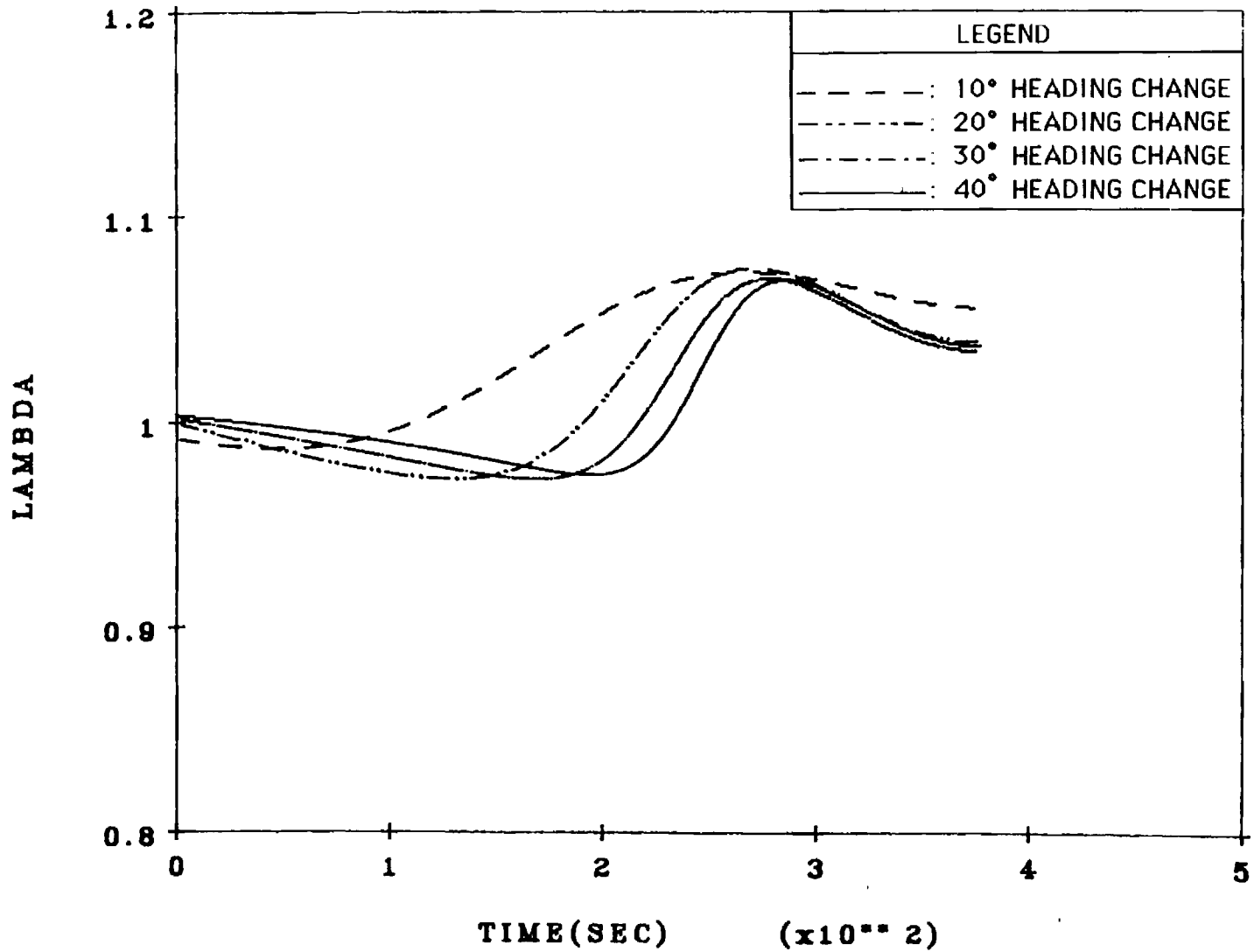


Figure 13. Optimal solution normalized lift coefficient profiles.

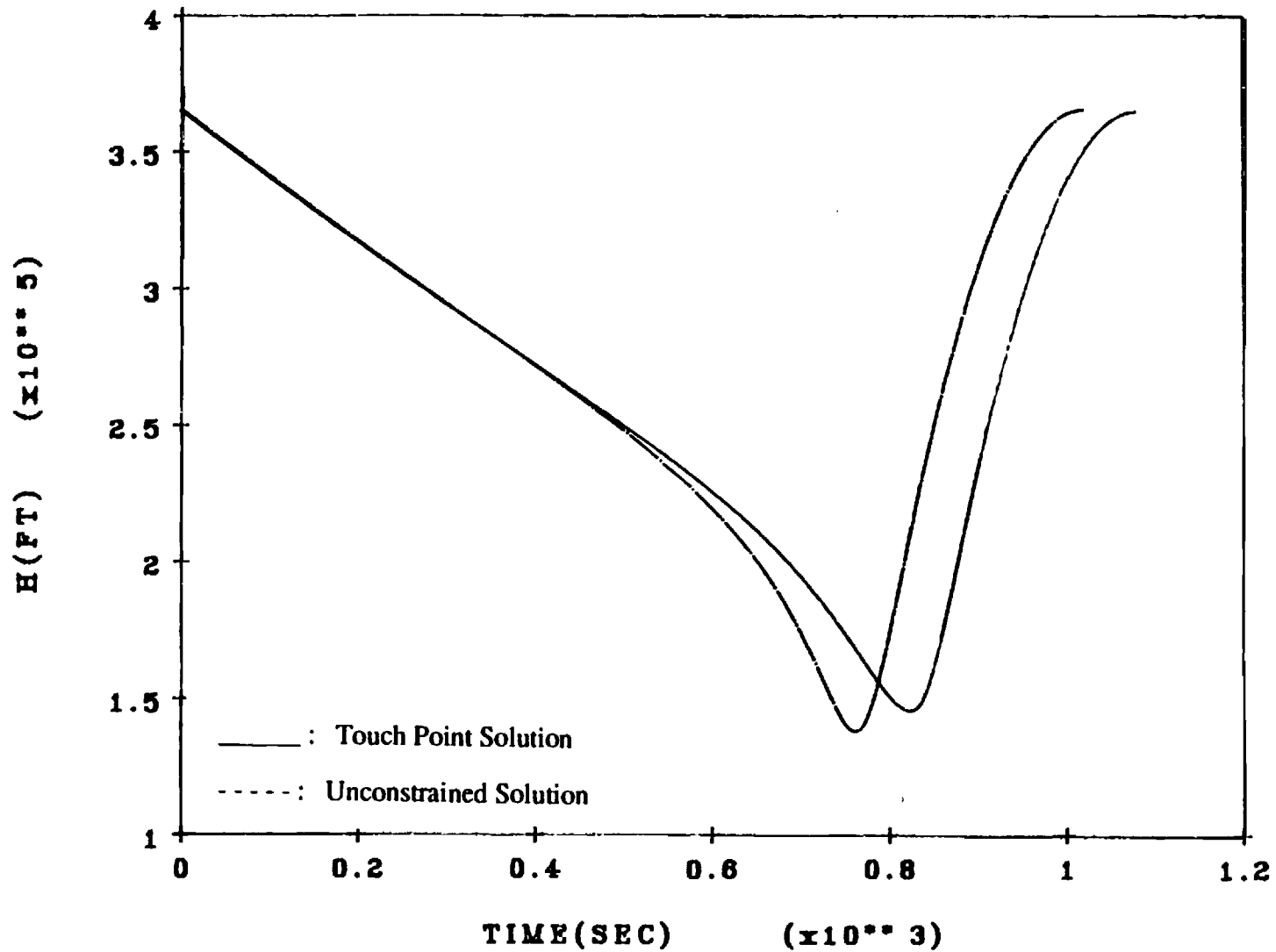


Figure 14. Altitude profiles for the unconstrained and touch point solutions.

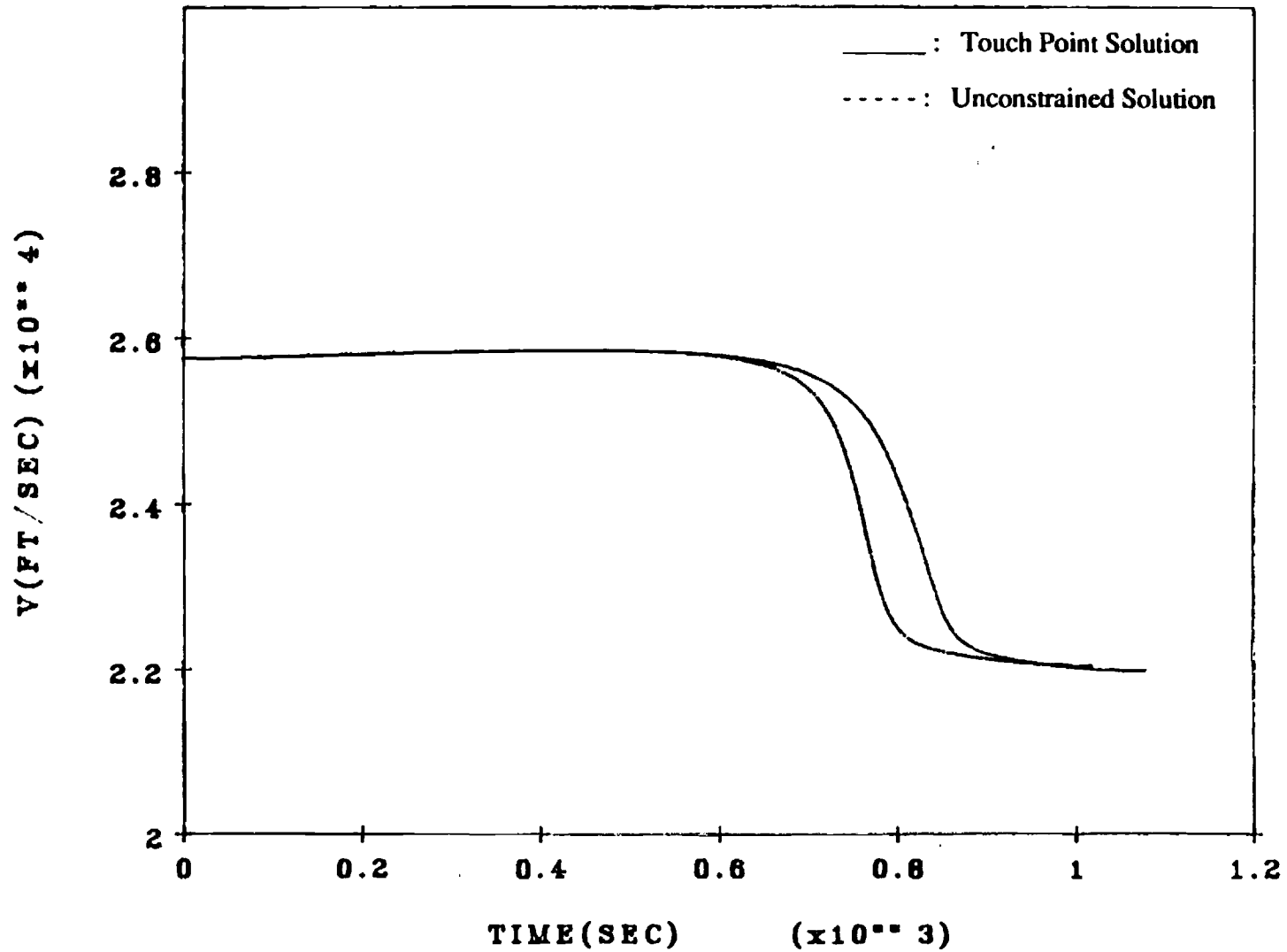


Figure 15. Velocity profiles for the unconstrained and touch point solutions.

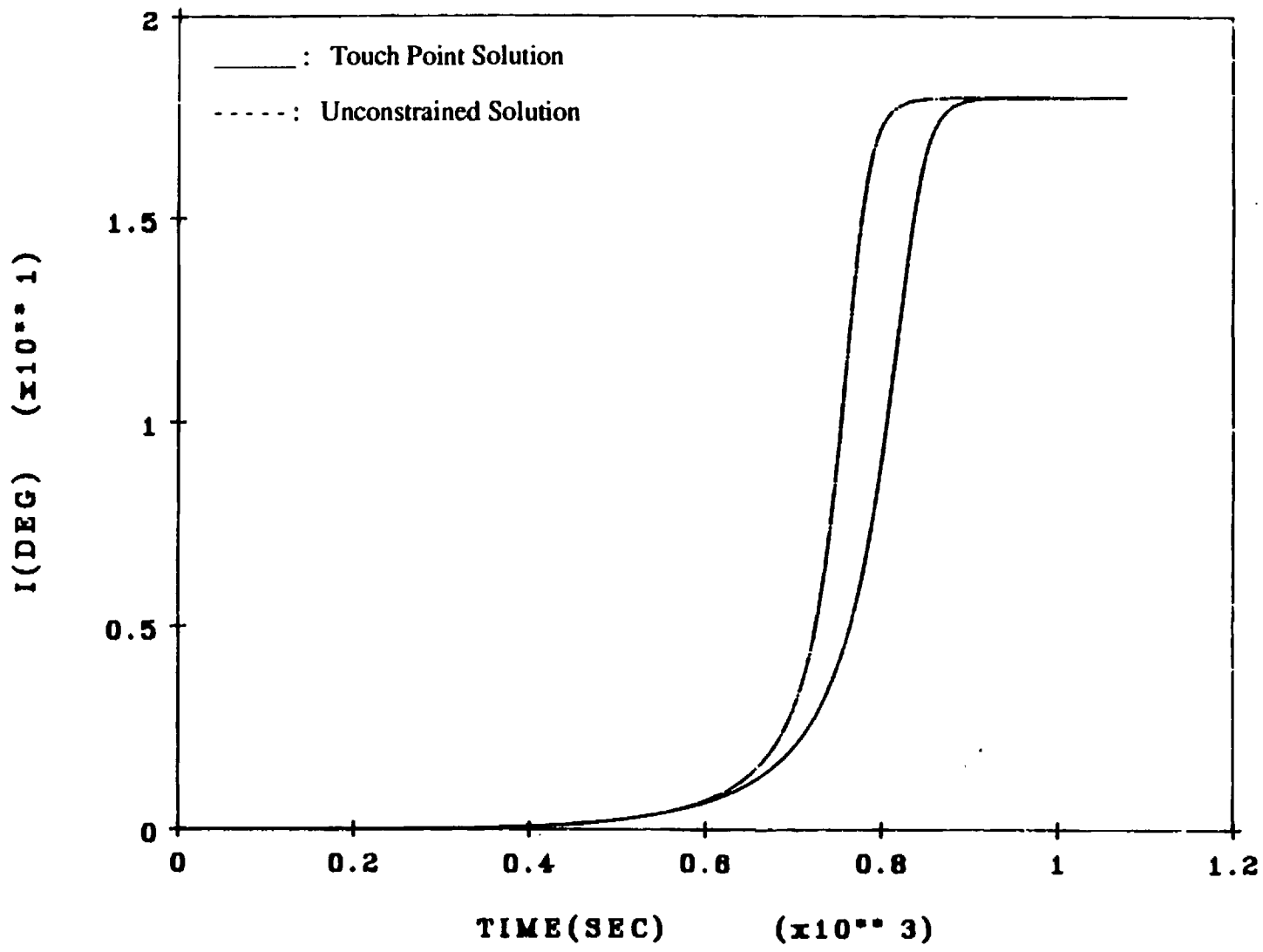


Figure 16. Inclination angle profiles for the unconstrained and touch point solutions.

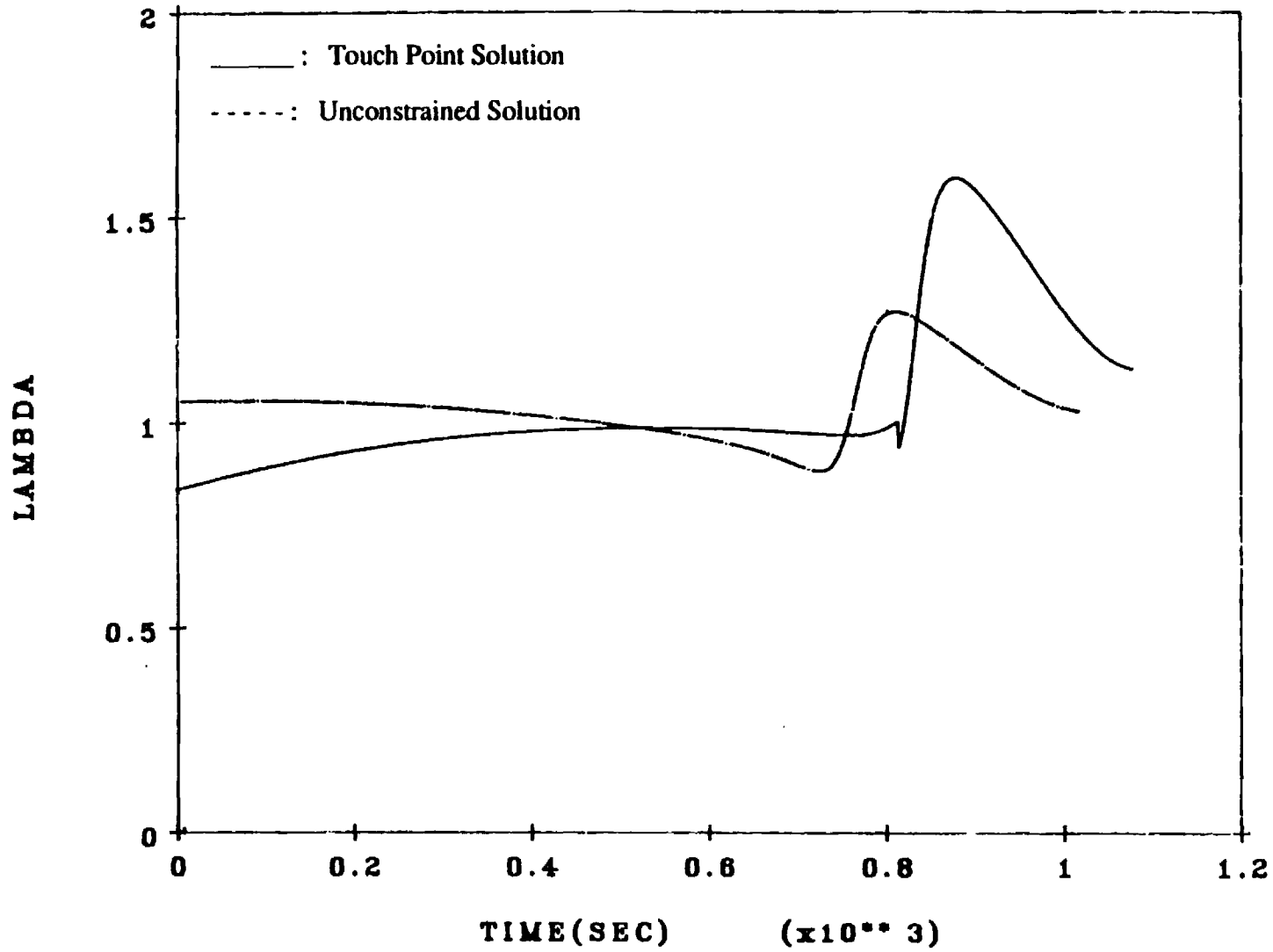


Figure 17. Normalized lift coefficient profiles for the unconstrained and touch point solution.

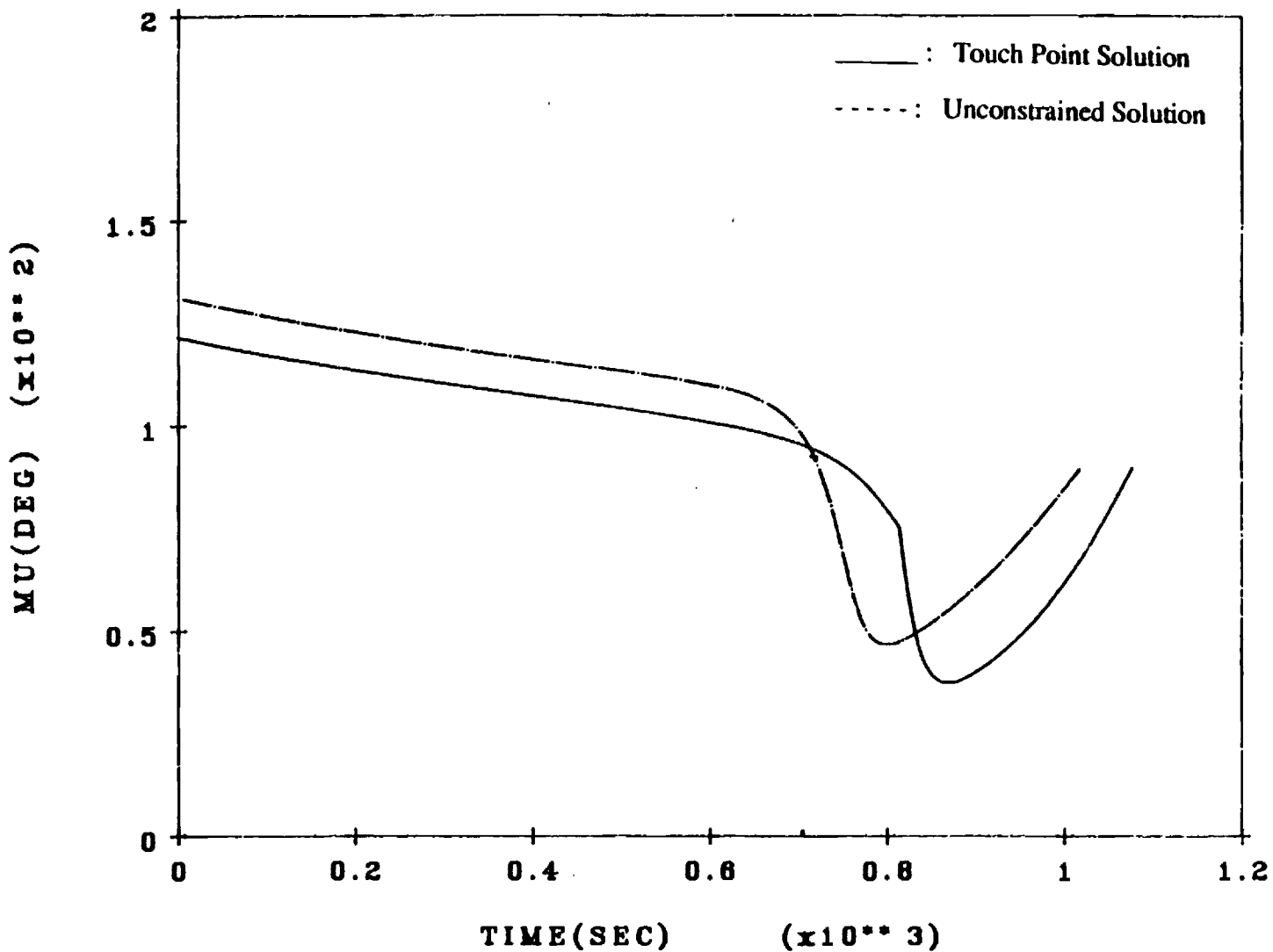


Figure 18. Bank angle profiles for the unconstrained and touch point solutions.

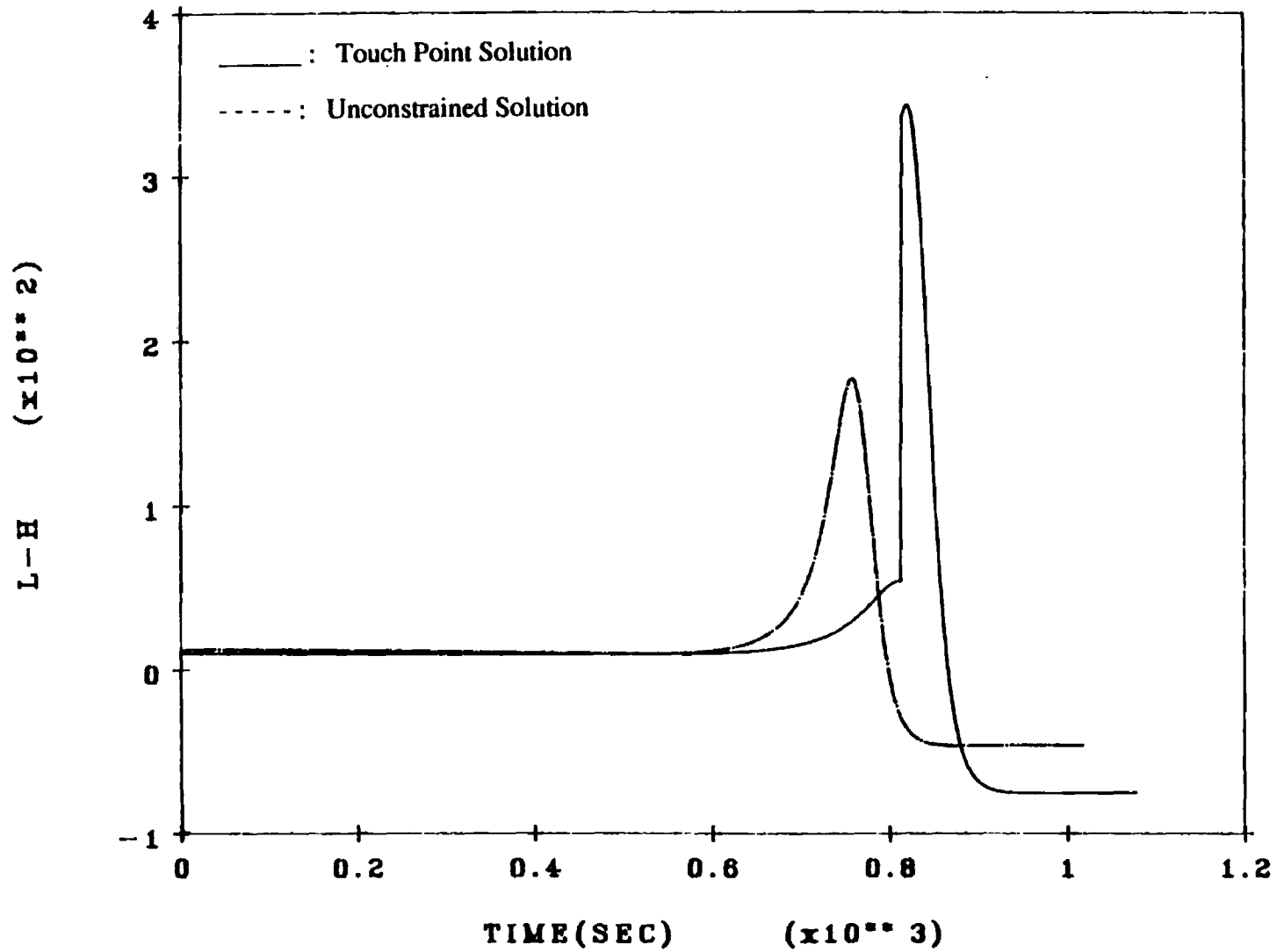


Figure 19. Altitude costate profiles for the unconstrained and touch point solutions.

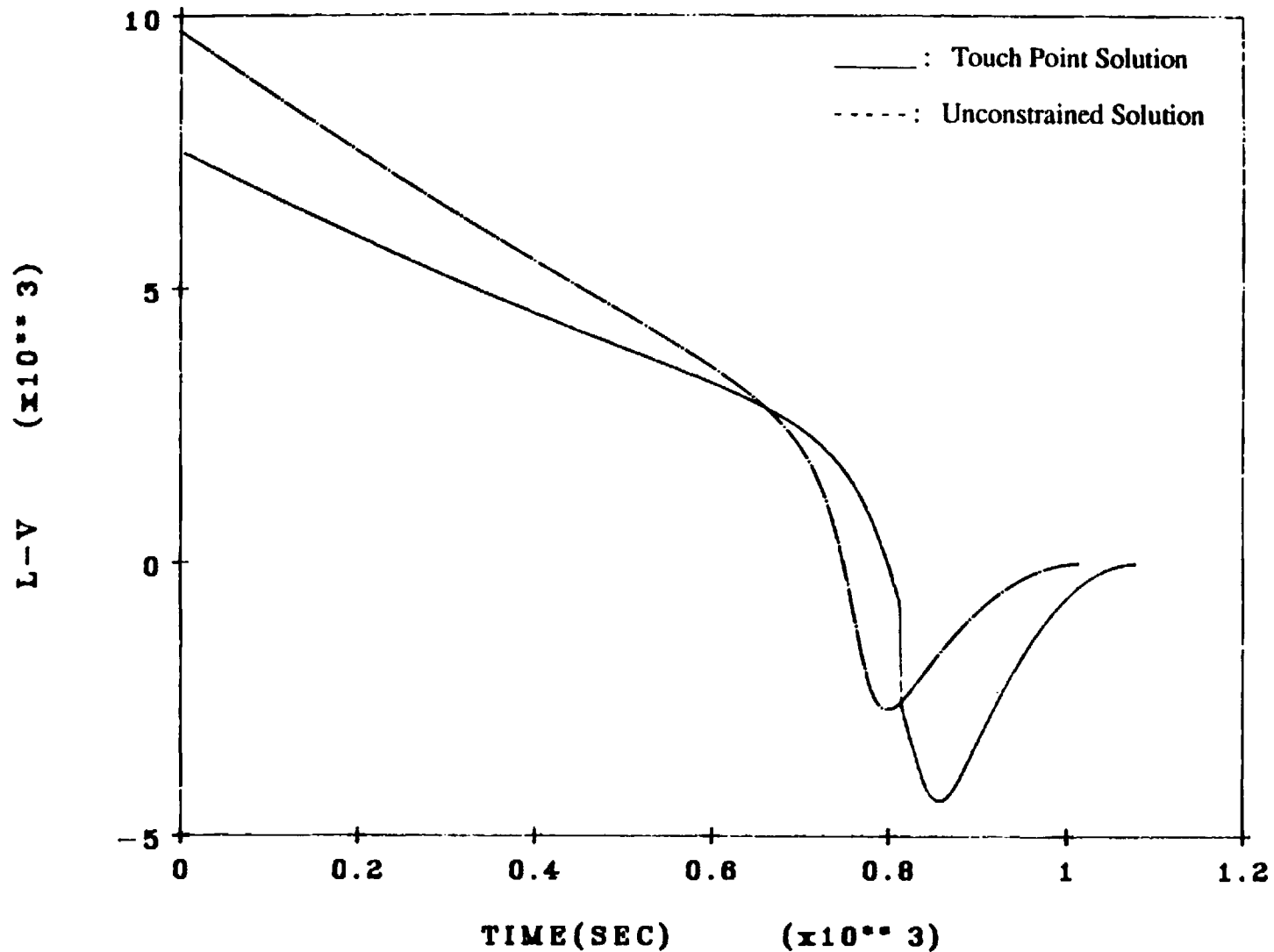


Figure 20. Velocity costate profiles for the unconstrained and touch point solutions.

Table 1
Comparison of Final Energies for the Reentry Problem

Guidance	Final Time	$E_f \times 10^8 (\text{ft}^2/\text{sec}^2)$	ΔE
Optimal	358.6	-4.813	1.510
SP1	397.0	-4.813	1.510
SP2	415.8	-4.814	1.511
SP3	398.0	-4.813	1.510

Table 2
Comparison of Energy Loss for the AOTV Problem

Heading Change	Optimal Solution $\times 10^7$	Guided Solution $\times 10^7$	% Error
10°	4.713	4.971	5.47
20°	8.858	9.109	2.83
30°	12.38	12.63	2.04
40°	15.40	15.66	1.69